SEARCHING FOR INFRARED EXCESSES AROUND WHITE DWARFS

by

Elin Deeb Wilson

A professional paper submitted in partial fulfillment
of the requirements for the degree

of

Master of Science

in

Science Education

MONTANA STATE UNIVERSITY
Bozeman, MT

July 2017

©COPYRIGHT

by

Elin D. Wilson

2017

All Rights Reserved

ACKNOWLEDGEMENT

I am extremely grateful to Dr. Luisa Rebull of IPAC at Caltech for her mentorship. I appreciate her guidance in designing and planning the project, the opportunity to spend a week at Caltech obtaining direct support, as well as her feedback throughout the writing process. Dr. Rebull was incredibly helpful with navigating and troubleshooting IDL programming.

I am also very thankful to Dr. John Debes of the Space Telescope Science Institute, who served as a consultant due to his expertise on dusty WDs. Dr. Debes provided project ideas and data, assisted with the modeling portion of this work, and provided feedback regarding SED interpretations as well as reviewed the final draft.

Dr. Chris Stark of the Space Telescope Science Institute obtained the FourStar data in 2013. He assisted with routines for processing the FourStar data.

I am thankful for the guidance provided by Dr. Walter Woolbaugh over the past year as a reader as well as course instructor. I am also thankful to Dr. Paterson for her help in formatting the final draft and answering formatting questions along the way.

I appreciate the willingness of my friend and colleague Jennifer Jones of Arapahoe Community College to also review the manuscript and provide feedback.

Finally, my husband Chris provided the support and encouragement that allowed me to pursue this program of study.

TABLE OF CONTENTS

1. INTRODUCTION 1

2. CONCEPTUAL FRAMEWORK 2

3. METHODOLOGY 11

4. DATA AND ANALYSIS 26

5. INTERPRETATION AND CONCLUSIONS 35

6. VALUE 49

REFERENCES CITED 51

APPENDICES 59

APPENDIX A: Target List with Coordinates 60
APPENDIX B: SED Plots 62
APPENDIX C: Model Parameters 71

LIST OF TABLES

1. Instrument/Survey Bandwidths and Resolution.....28

2. FourStar Photometry.....32

3. χ Calculations.....37

4. IR Excess Due to Source Confusion.....41

5. WD+BD Candidates.....42

6. Disk Candidates.....45

7. Target names with Coordinates (Appendix A).....61

8. Model Parameters (Appendix C).....72

LIST OF FIGURES

1. Sirius A with WD Sirius B 4

2. Photometry of GALEX1931+0117 by Debes et al. (2011) 10

3. Absolute vs. Apparent Magnitude 13

4. Filter transmission curves for J, H and Ks IR bands.....15

5. Blackbody Curves.....17

6. Characterizing SEDs and IR Excesses.....18

7. Face on Mars (resolution example).....22

8. Plot of flux density vs. wavelength for SDSS J03030835+005443.7.....23

9. Spectral Classifications (N=66) 27

10. Percentage of Sample With Data Available From Each Survey (N=66).....29

11. Presence of an Excess (N=66) 36

12. SED for 153149.04+025705.0 (IR excess due to source confusion).....38

13. RB Image for 153149.04+025705.0 (IR Excess due to source confusion) 38

14. SED of WD 1929+012/GALEX J1931+0117 39

15. RGB image of WD 1929+012/GALEX J1931+0117.....39

16. RB Image for WD 0106-328 (IR excess plus source confusion).....40

17. SED of WD 0106-328 (IR excess plus source confusion).....40

18. RB Image for 231725.28-084032.9 (WD+BD candidate).....43

19. SED for 231725.28-084032.9 (WD+BD candidate) 43

20. SED for WD 2115-560 (known dusty) 44

21. RB Image for WD 2115-560 (known dusty) 44

22. SED for 161717.04+162022.3 46

23. SED for GD 153 (non-dusty, calibration star) 47

24. SED of PG 1457-086 47

ABSTRACT

Many white dwarf stars (WDs) have been found to be "polluted," meaning they contain elements heavier than hydrogen and helium in their atmospheres. One proposed external mechanism for atmospheric pollution of cooler WDs is the accretion of rocky bodies. Disintegration of rocky bodies (formerly planets, asteroids etc.) would leave a circumstellar (CS) disk of debris that would then accrete onto the WD, "polluting" the atmosphere. When heated, CS disks emit excess infrared (IR) light. WDs with IR excesses suggestive of a CS disk are known as dusty WDs. Statistical studies are still needed to determine how numerous dusty, polluted WDs are, along with trends and correlations regarding the rate of planetary accretion, the lifetimes of CS disks around WDs, and the structure and evolution of WD CS disks. A sample of 39 WD stars were initially identified as containing IR excesses based on WISE data as part of the WISE InfraRed Excesses around Degenerates (WIRED) Survey (Debes et al. 2011). Data for these along with 27 additional targets was acquired by the FourStar Infrared Camera Array. Archival optical and IR data from WISE, Spitzer, 2MASS, DENIS, SDSS, PanSTARRS, and UKIDSS were used to create spectral energy distributions (SEDs) to search for excesses. FourStar data are much higher spatial resolution than the WISE data initially used to select the WIRED candidates, and thus can indicate if an apparent excess is due to a nearby companion vs. a CS disk. Seventeen WDs look to have CS disks, 7 of which are newly identified, ten of which are known to be metal-rich. Ten additional targets have an excess, but these are likely due to a BD companion, 7 of which are new detections, 1 of which also has an excess from source confusion. Eleven targets had excesses resulting from source confusion, including 3 that are still considered disk candidates and 1 WD+BD candidate. Thirty targets were determined to not contain an excess, one of which in literature was thought to contain an excess, two of which are metal-rich. Two targets were determined not to be WDs after all.

INTRODUCTION

When stars up to 8 times the mass of our Sun die, they shed their outer layers, forming a planetary nebula, revealing a white dwarf (WD) in the center. The WD is the remnant of what used to be the core of the star. WDs are compact objects; they have masses up to 1.4 times that of our Sun within a radius comparable to Earth's. Elements heavier than H and He should sink to lower layers; however, between 25%-50% of WDs have been found to be "polluted," meaning they contain elements heavier than H and He, such as Ca, Si and Fe, in their atmospheres (Xu & Jura, 2012; Koester, Gänsicke & Farihi, 2014; Zuckerman, Keister, Reid & Hünch 2003; Zuckerman, Melis, Klein, Koester & Jura 2010). Any small quantities of these heavier elements should sink below the WD outer layers on relatively short timescales (days to millions of years), so for a long time, there was no explanation as to why some WDs were polluted. One proposed external mechanism for atmospheric pollution of WDs is the disintegration of rocky bodies (e.g. planets, asteroids, dwarf planets) due to the tidal forces present around WDs, leading to accretion of heavier elements onto the atmospheres of these WDs. Disintegration of planetary bodies would result in a circumstellar (CS) disk of debris. As CS disks are heated by the WD, they emit excess infrared (IR) emission, meaning a WD target with excess IR emission potentially has a CS disk of disintegrated planetary remains (Zuckerman, 2001). These are known as "dusty" WDs, the first of which was discovered in 1987, and up until recently only a few additional dusty WDs had been discovered (von Hippel, Kuchner, Kilic, Mullally & Reach, 2007).

Statistical studies are still needed to determine how many polluted WDs are dusty, along with planetary accretion rates, WD CS disk lifetimes, and the structure and evolution of these disks (Debes et al. 2011). These findings will allow for a better understanding of the fates of planets that survive the giant phases of their stars. The research goal of this study is to determine how many targets in a sample of 66 WDs contain IR excesses, as well as the potential sources of these excesses (whether a CS disk is likely present, or a nearby companion is the source of excess).

CONCEPTUAL FRAMEWORK

Stellar Evolution and WD Formation

A star's life cycle is governed by a battle of two forces: gravity (in) and internal pressure (out) (Bennett, Donahue, Schneider & Voit, 2009). The longest and most stable stage is known as the main-sequence (MS) stage, during which thermonuclear reactions in the core fuse H nuclei into He nuclei, and pressure from fusion counters the force of gravity. Currently, the Sun, an intermediate mass MS star, is about half-way through its 10 billion-year lifetime. Lower mass stars (typically less than 0.5 solar masses or $M_{\odot}$) will not become hot enough to fuse other elements in the core. But stars of intermediate mass like our Sun, upon exhausting the H in their cores, will experience core gravitational collapse until the core reaches a temperature sufficient to allow for ignition of He to C fusion. Other layers outside the core that are sufficiently hot and dense will undergo H to He fusion as well. The combination of core He fusion and a surrounding layer of H fusion leads to an increase in internal pressure, which causes the outer layers

of the star to expand and cool; this stage is known as the red giant (RG) phase. Our Sun will “swallow” Mercury, Venus, and possibly Earth in this phase. Over time, the outer layers of the RG are shed, forming a planetary nebula (which is poorly named, because it has nothing to do with planets).

Eventually fusion within the core of a star will cease once the fuel (e.g. H or He) runs out; exactly which fuel and exactly when this happens depends on the star's mass. Gravity collapses the star now that pressure from fusion cannot counter it, making the core denser and denser, forming an electron degenerate remnant called a white dwarf (WD) star. In a WD, electrons exert an opposing pressure to gravity known as electron degeneracy pressure. Electron degeneracy pressure results from the Pauli Exclusion Principle, which states that two electrons of the same spin cannot occupy the same quantum state. The outer layers of the star crash down on this remnant, but the WD cannot be compressed any further, so the outer layers "bounce" off the core and are ejected. WDs composed primarily of carbon (C WDs) cool into a “diamond-like” structure (Metcalfe, Montgomery & Kanaan, 2004), and WDs composed primarily of He (He WDs) may form a state of matter resembling a Bose-Einstein condensate (Bedaque, Berkowitz & Cherman, 2012). Because of gravitational collapse, WDs have masses comparable to the Sun’s mass squished into a volume equivalent to Earth’s radius. Counterintuitively, the more massive the WD, the smaller the radius. A teaspoon of WD material could therefore weigh approximately 5 tons (Bass, 2014). Sirius B for example, which is the closest WD to Earth and a companion to the bright star Sirius A (Figure 1), contains a mass similar to that of the Sun (0.98 $M_{\odot}$) confined to a radius smaller than

Earth's (HubbleSite, 2005). This extreme density causes strong gravitational tidal forces. As mass increases, electron velocities also increase in order to continue to oppose the increase in gravity while still being governed by the Pauli Exclusion Principle. Subrahmanyan Chandrasekhar first determined this results in an upper mass limit to WDs, since electrons contain mass and thus cannot attain the speed of light (Thorne, 140-159). Accounting for relativity, the Chandrasekhar limit for He and C WDs is 1.397 $M_{\odot}$, and 1.2 $M_{\odot}$ for Fe WDs, with others falling between these values (Mathew & Nandy, 2014). WDs that accrete material from a binary companion can undergo surface H fusion, appearing as a nova. If a WD near the Chandrasekhar limit accretes enough matter from a companion star, it will become unstable and explode as a Type I supernova.

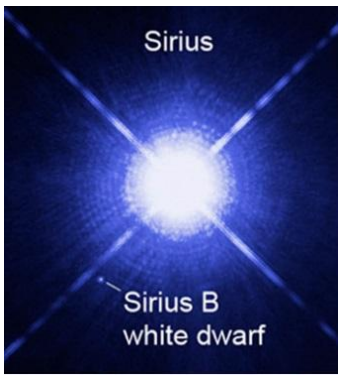


Figure 1. Sirius A and B. Sirius A is a MS star of about 2 $M_{\odot}$, Sirius B is a WD with a mass comparable to the Sun's, but a radius less than Earth's. Credit: HST image, NASA, ESA.

Stars more massive than 8 $M_{\odot}$ face different fates. They undergo more fusion processes up to iron, and the increased mass, greater force of gravity and inability to fuse iron causes the cores of these stars to collapse into a neutron star, in which neutron degeneracy pressure opposes gravity and the object is simply a mass of neutrons. If more

than about 2.9 $M_{\odot}$ remains in the core, gravity "wins" and a black hole forms (Chamel, Haensel, Zdunik & Fantina, 2013). In this work, we are concerned solely with WDs.

Classification and Characteristics of WDs

WD stars are primarily composed of He or C, although heavier elements such as O, Ni, and Fe may be present depending on the initial star's mass and resulting thermonuclear reactions that took place in the parent star. They are classified by absorption lines in their spectra, which result from both temperature and composition. Designations begin with the letter "D" for "degenerate," followed by a letter indicating spectroscopic signatures:

- DA-Hydrogen lines ($5000K<T_{eff}<80000K$)
- DB-He I lines ($T_{eff}<30000K$)
- DC-Continuous spectrum ($T_{eff}<11,000K$)
- DZ-Metal lines (Mg, Ca, Fe)
- DQ-Atomic/Molecular carbon features
- DO-He II lines ($T_{eff}>45,000K$).
- DH-Magnetic fields

Additional letters indicate additional features, e.g. a DAB WD has strong H lines as well as weaker He lines. A DAZ WD has prominent H lines as well as metal lines. Other variations that may exist include variability (denoted with a V), or magnetic properties (P=polarized magnetic; H=non-polarized magnetic) (Hoard, 2011; Sion, Greenstein, Landstreet, Liebert, Shipman & Wegner 1983). DZ stars are candidates for atmospheric

pollution; most known polluted WD stars have a DZ classification (including DAZ, DBAZ, DBZ).

Due to high surface gravity, the material of a WD no longer behaves as an ideal gas. Differentiation takes place, in which heavier elements sink to the core and H and He remain as a thin atmosphere. This process is known as gravitational settling, and it should happen on relatively short timescales. Surprisingly, approximately 25% of DA WDs (those with hydrogen dominated atmospheres) and 33% of DB WDs (those with helium dominated atmospheres) contain heavier elements in their atmospheres (Zuckerman et al. 2003; Zuckerman et al 2010; Xu & Jura, 2012). Since gravitational settling should occur relatively quickly, it is surprising that so many WDs are polluted, suggesting that these heavier elements need to be replenished. Warmer "polluted" WDs have been found to contain signs of CS disks (or to be "dusty"), but cooler polluted WDs have been found to not be dusty. One proposed mechanism for these observations is that dust from disintegrated planets is accreted onto the WD's surface, with a high accretion rate being responsible for the absence of CS disks around cooler WDs (Xu & Jura, 2012). Cooler WDs are likely older, so they have potentially depleted the CS disk. Another potential component for metal enrichment in really hot DA WDs (T_{eff}>17000 K) is that in addition to accretion, radiative levitation might account for the presence of certain elements such as silicon. Radiative levitation essentially results from ionization of these elements; pressure from the radiation (out) counters the gravitational pressure (in). Radiative levitation may be a secondary source of atmospheric pollution, if not a primary source in

some targets (Chayer, 2013); however, this can only occur at certain temperatures, and for lighter elements.

The Fates of Planets

During the RG phase, a star's radius becomes much larger than it was during the MS phase (50-100 times the MS radius of the star). The Sun's outer layers for example may extend to almost the distance of Earth, known as 1 astronomical unit (1 AU). Inner planets can (and will) be ingested as stars expand into RGs. Computer simulations indicate that the shedding of material from the outer layers combined with shifting tidal forces from the star can impact the orbital positions and stability of other remaining planetary bodies. A star like the Sun will likely clear a radius of up to 2 AU of all planetary bodies (past Mars), and larger stars can clear up to 5 AU. Interactions between planetary bodies can then add to the disruption, leading to collisions, ejection of some objects, and/or scattering of surviving bodies into eccentric orbits. The degree of disruption and scattering depends on the number of objects, the location of objects, as well as the masses of the objects present in the system. Objects that are scattered closer to the star can be tidally torn apart, leading to the formation of a CS disk. Continued disintegration can result from the tidal forces of the remnant WD, which may then accrete some of the rocky material. Accretion of planetary debris is thus proposed to be the primary source of a WD's atmosphere becoming polluted (Mustill, Villaver, Veras, Bonser & Wyatt, 2013; Debes & Sigurdsson, 2002).

Examples of Dusty, Polluted WD Stars

The first metal-rich WD to be discovered to have an IR excess is G29-38. A substantial emission between 2 and 5 μm was discovered in 1987 by Zuckerman and Becklin, who initially hypothesized the excess to be caused by a brown dwarf (BD) companion. BDs are sometimes called "failed stars" because they do not have enough mass to ignite H fusion in their cores. In some ways, BDs are similar to the gas giant Jupiter, but are more massive and thought to form in a different way than planets form. A BD was not detected, however, around this WD (Kuchner, Koresko & Brown, 1998), meaning the excess was attributed not to a companion, but to a dusty CS disk; the source of the disk, however, continued to remain a mystery. Three explanations for the presence of the disk were proposed: (1) the WD was embedded in an interstellar cloud and material had been drawn into a disk; (2) a “cosmic catastrophe” in which two massive objects collided and shattering had occurred; or (3) due to material from an unseen companion being pulled in (Zuckerman 2001). More recent observations support planetary debris as the source of a disk (Reach et al., 2005; Debes & López-Morales, 2008).

The launch of telescopes such as Hubble (particularly with the upgraded addition of the Cosmic Origins Spectrograph or COS), the Wide-field Infrared Survey Explorer (WISE; Wright et al., 2010), the 2-Micron All Sky Survey (2MASS; Skrutskie et al., 2006), and Spitzer Space Telescope (Werner et al., 2004) have since allowed for higher-sensitivity observations of WDs, resulting in the discovery of a large number of dusty WDs that are known to be polluted, and archives of data that probably contain more

waiting to be discovered. It seems the dust, including the debris around G29-38, is in fact coming from disrupted planets. By continuing to search for and study debris disks around WDs, researchers can gain additional insight into the planets' orbits, composition, the post-MS evolution of stars, timescales for disk formation, the potential formation of second-generation planets, and dust formation physics in general (Debes et al. 2011).

GALEX J193156.8+011745 (GALEX1931+0117) is an example of a DAZ-classified white dwarf with elements such as Mg, Si, O, Ca, and Fe present in the atmosphere. Previous studies found an IR excess, Debes et al. (2011) as well as Melis et al. (2011) determined the IR excess to be due to a disk. UV through IR data was used to determine the flux energy distribution as a function of wavelength. Debes et al. (2011) detected an IR excess at 3.4 and 4.6 μm; modeling indicates this excess arises from a dust ring within the tidal disruption radius of the WD (Figure 2). The excess, along with metals present in the spectrum of this particular object, suggest a rocky body that was once an Earth-mass planet has been disrupted and is accreting onto the WD.

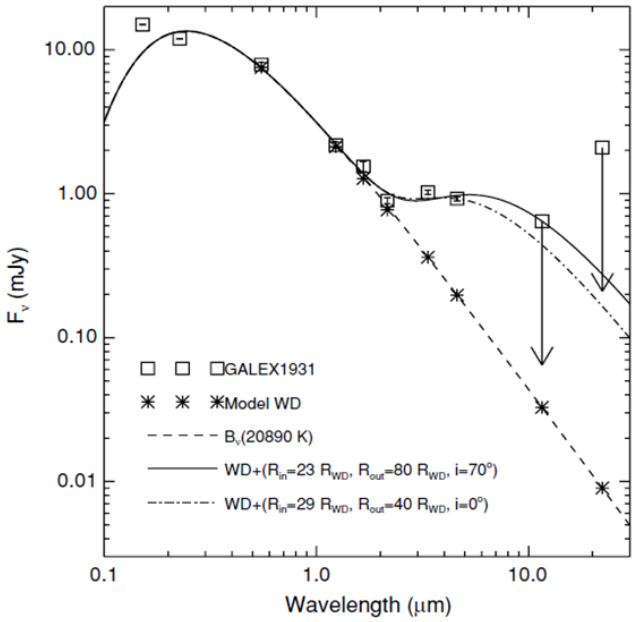


Figure 2. Flux energy distribution of GALEX1931+0117 by Debes et al. (2011, p.7). The model of the WD alone is the asterisks and dashed line. There is a larger flux energy at IR wavelengths than expected from the WD alone. The model that best fits the data includes a dust ring stretching from 29 R_{WD} to 40 R_{WD}.

WD 1145+017 made news headlines as a “planet destroyer” (O’Neill, 2015). Vanderburg et. al. (2015) determined this object contains metal lines in its atmosphere and evidence of actively disintegrating dwarf planet pieces. They used the transit method this by examining data taken over a period of 80 days from a multitude of instruments. Characteristics of the transits (asymmetry/variations in the period) indicate a chaotic system that cannot be attributed to standard variations in the target’s brightness, or to an orbiting stellar companion or BD. Spectra indicate the debris consists of metals such as Mg, Al, Si, Fe and Ni.

METHODOLOGY

Important Concepts and Units

Photometry

Photometry is the technique of quantitatively measuring the brightness of an object in an image, or, the quantity of electromagnetic (EM) radiation recorded by the detector from that object or objects. Since the 1980's, most optical astronomical data are typically collected using charge couple device (CCD) cameras, which convert light detections into electrical charges. A CCD has a series of semiconductor capacitor cells known as pixels. These pixels are much like "buckets" for collecting light. The charges generated are transferred from the chip, producing a reading for each pixel in terms of photon counts. IR data are similarly obtained by detectors that convert photons to electrons (although these are not technically CCDs). The resulting measurement can be converted to units of flux. Flux is energy per unit area per unit time, e.g., J/cm^2/s in SI mks units, or ergs/cm^2/s in cgs units; and flux density is flux per photon in a sense. The astronomy-specific unit "Jansky" is a flux density unit equivalent to 10^{-26} Watts/m^2/Hz. Hz is the SI unit for frequency of EM radiation, which is inversely proportional to wavelength ($c = \lambda\upsilon$, where c = the speed of light which is 2.99×10^8m/s, λ = wavelength in m, and υ = frequency in Hz). The unit "watt" is the SI unit for power, which is energy/time (Joules/second), so a Jy is equivalent to J/s/m^2/Hz, meaning a unit of energy/time/area/photon frequency.

Sometimes photometric data are reported as limits, in which we know there is a source there from observations at other bands, but the source is not detected with any

significance at that band (e.g. W3 and W4). Thus, photometry is done on the blank sky at that location as if the source were detected, and a measure of the scatter in that region is obtained. Typically, three times the scatter is taken as the limit, as we do not know what the true brightness is at this band from these data, but we know it must be fainter than this measurement, otherwise we would have detected it.

The Magnitude System

The brightness of objects in astronomy are also measured in terms of magnitude, which is a brightness unit based on an ancient Greek scale developed by Hipparchus in which 1st magnitude stars were the brightest, 2nd magnitude stars were second brightest, etc. Thus, the larger the number, the dimmer the object. This definition needed to consider factors like physical size and distance, so we now differentiate between apparent magnitude (based on what we see here on Earth) vs. absolute magnitude (how all objects would compare in brightness if they were all found at a distance of 32.6 light years; a light year is a unit of distance, equal to 9.461 trillion km). For example, the Sun's apparent magnitude is -26, but if distance is accounted for, its absolute magnitude is about +5. Certain stars like Vega are used as standards, which are defined to have an absolute magnitude of 0. The dimmest stars seen in rural areas correspond to a magnitude of 6. A single magnitude difference corresponds to a factor of ~2.512 in brightness, meaning 5 magnitude steps is a factor of 100 (so a magnitude 5 star is 100 times dimmer than a magnitude 0 star) (Bennett et al. 2009, p. 523-524).

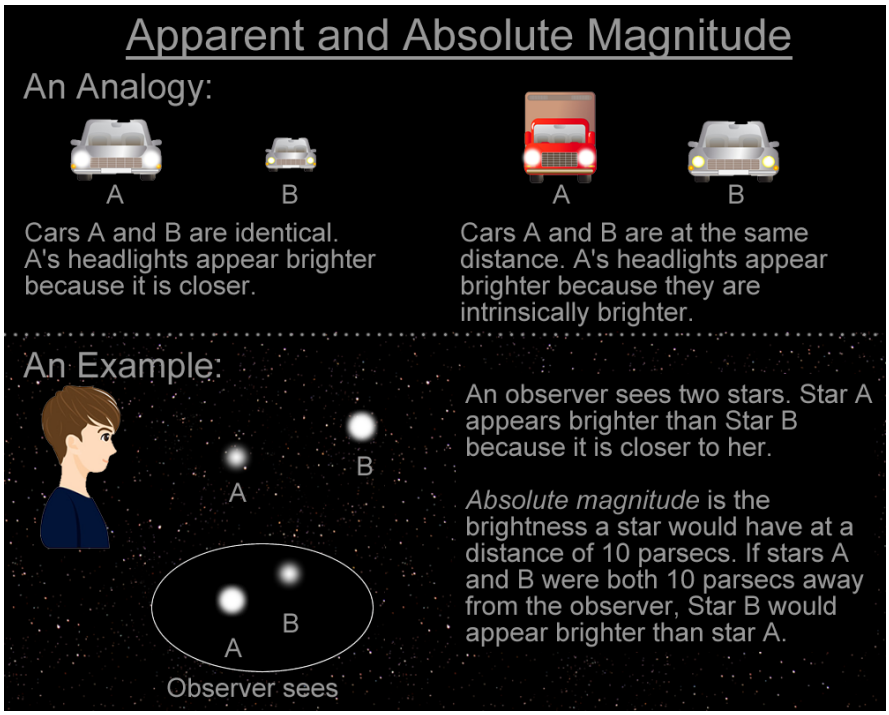


Figure 3. Absolute vs. Apparent Magnitude. The difference between apparent and absolute magnitude is that apparent magnitude is based on how things appear from Earth, whereas absolute magnitude examines what we would see if all objects were the same distance away. This can be used as a distance determination method. Credit: https://lco.global/spacebook/what-absolute-magnitude/

Reducing Photometric Data

To reduce CCD data, one takes a series of calibration frames to remove the pixel-to-pixel variations and other instrumental noise. To do photometry, or calculate the quantitative brightness of an object, one must measure the brightness of the object and subtract off the brightness of the sky background near the object. This is especially important for optical Earth-based instruments—the sky contribution comes from atmospheric effects and city lights, known as “light pollution.” It can be important for space-based missions too; the background near the target may be fairly bright if it is seen

through diffuse emission from dust/gas in our Solar System, in amongst dust/gas near the object, or superimposed on dust/gas behind the target object.

With a single image, photometric data can be obtained for many objects at once. Many large-scale surveys set out to image a significant fraction of the sky; these large-scale surveys deliver the photometry as part of their project. As a result, especially in the last 5-10 years, many photometric catalogs (across many wavelengths) have become available to the community.

Photometric data is typically acquired over a relatively small range of wavelengths for each image. Filters isolate specific wavelength bands (Figure 4). One can think of filters as colored cellophane, e.g. red cellophane only allows red light through. Astronomical filters are more sophisticated than cellophane, though, and can be used at all wavelengths from radio to gamma rays.

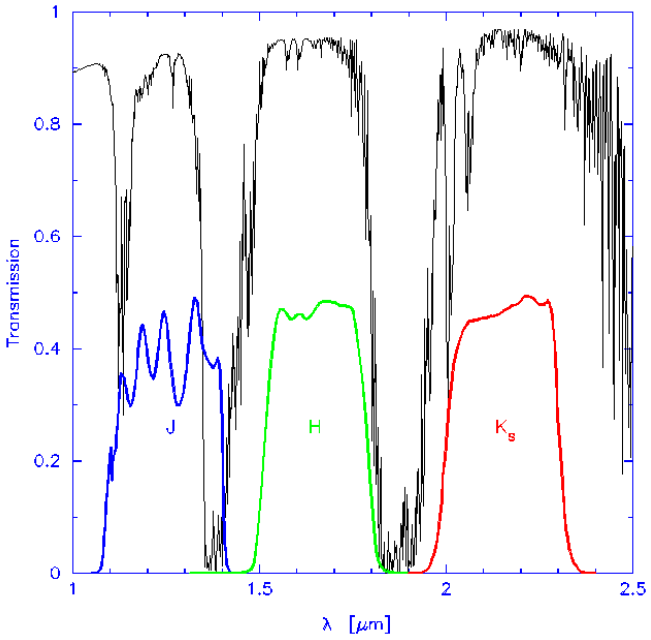


Figure 4. Filter transmission curves as a function of wavelength in microns, from the 2MASS documentation (http://www.astro.caltech.edu/~jmc/2mass/v3/transformations/) for J, H and K_s IR bands, which are found on instruments such as UKIDSS, FourStar, and 2MASS. The black line is the transmission of Earth's atmosphere for comparison. These filters are specifically placed in regions of high atmospheric transmission to enable ground-based observation in the IR. Only certain wavelengths are allowed through each filter bandpass.

Blackbodies and SED curves

Any object that has a temperature and density (you, your dog, the Sun, the Universe) emits light that can be described by a blackbody (BB) function. The function is expressed as

$$B_\lambda = \left(\frac{\frac{2hc^2}{\lambda^5}}{e^{\frac{hc}{\lambda kT}} - 1} \right),$$

where h = $6.6260755 \times 10^{-27}$ erg*sec, c = the speed of light = 2.997924×10^{10} cm/sec, T = temperature in Kelvin, and k = 1.380658×10^{-16} erg/deg. A common everyday example of a BB is an old-fashioned lightbulb with a filament or an oven burner. The

hotter an object, the brighter the light and the shorter the peak wavelength (meaning that the peak of the emission becomes bluer)—this is known as Wien's Law, $\lambda_{peak}\ (\mu m) = \frac{2900}{T}$, where λ_{peak} is peak wavelength in micrometers (microns) and T is temperature in Kelvin. A star like the Sun (T~5800 K) peaks at about 0.500 μm, which is in the green portion of the visible spectrum; hotter stars peak towards the blue portion of the spectrum, cooler stars peak in the red portion of the spectrum. BDs and planets are cool enough that they peak in IR, as do lightbulbs (this is in fact why filament lightbulbs are so inefficient compared with LEDs and CFLs; filament lightbulbs emit mostly energy we cannot even see). The hotter the target, the brighter it is across all wavelengths (see examples in Figure 5), this is known as the Stefan-Boltzmann Law in which $E \propto T^4$, where E = energy and T = temperature. Most WDs have much hotter surface temperatures than the Sun (particularly H dominated DA WDs), although as they cool, their spectra will change over time, becoming cooler and redder, until they eventually remain as black dwarfs (which takes an extremely long time).

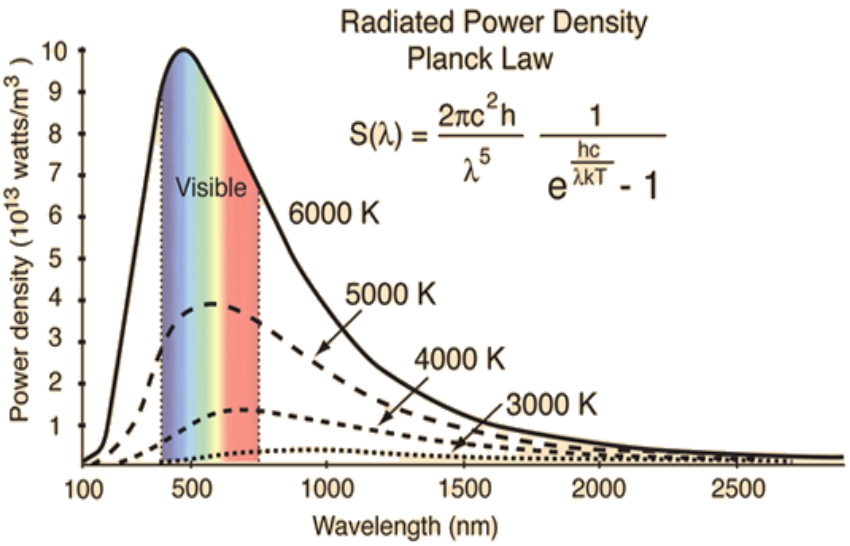


Figure 5. Sample blackbody curves based on Planck's Law. The 6000K curve corresponds to temperature of the Sun, 3000 K corresponds to the temperature of a lightbulb filament. Hotter targets emit more radiation, across more wavelengths, and peak at shorter wavelengths (higher energies).
Credit: http://hyperphysics.phy-astr.gsu.edu/hbase/bbrc.html

If a CS disk is present around a WD, this dust will intercept some of the radiation from the WD, causing the CS disk to heat up and remit energy at IR wavelengths – generating more radiation in the IR portion of the spectrum than is expected for a dust-free solitary WD. This will alter the shape of the emission from the star (Figure 6).

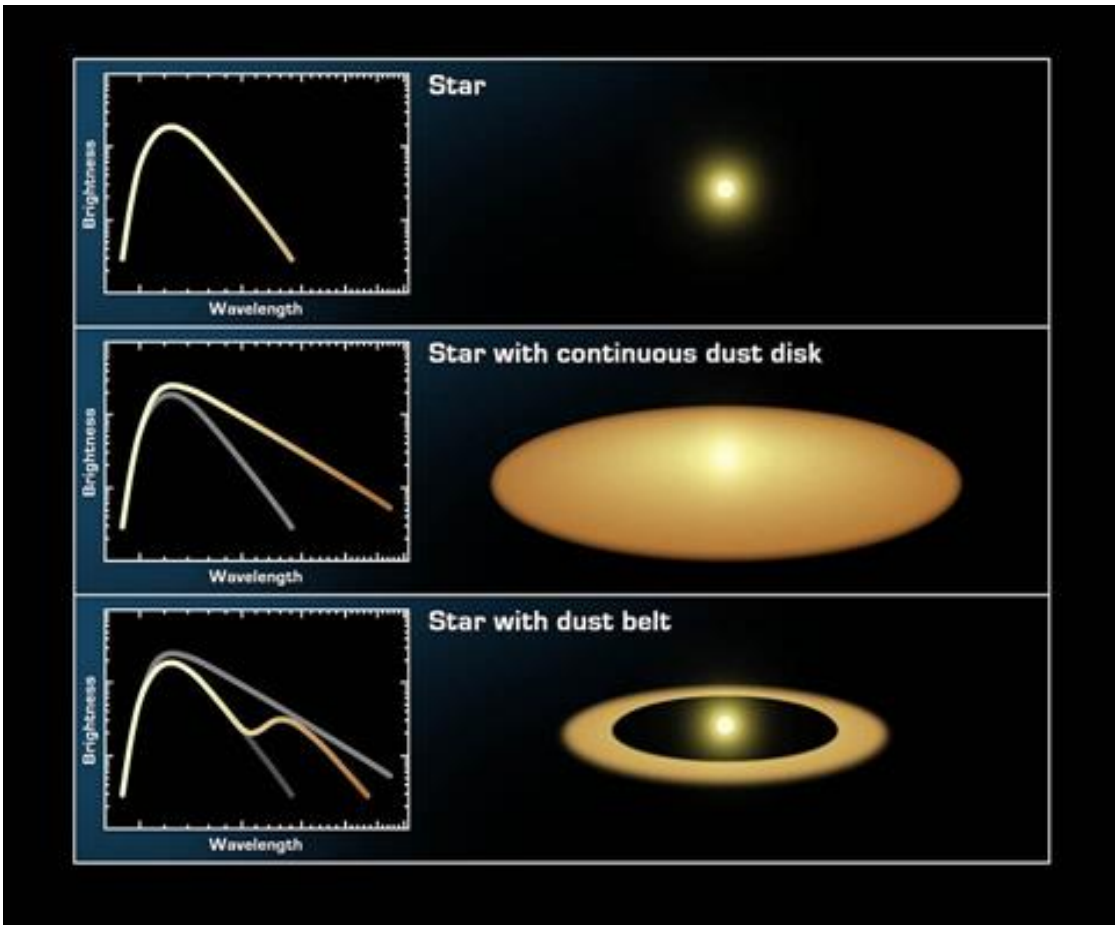


Figure 6. As a circumstellar disk or shell surrounding a star is heated, energy is re-emitted at IR wavelengths. When more IR energy is emitted than is expected from a stellar photosphere, this is called an "IR excess." The top SED corresponds to a "naked" star. The middle SED represents what the data would show if a continuous disk is found around the star—more radiation is being given of at IR wavelengths than the star would give off on its own. The last SED corresponds to what an object with a dust belt (or ring) would exhibit, similar to what Debes et al. (2011) found for GALEX1931+0117 (Figure 2). Credit: NASA/JPL-Caltech/T. Pyle (SSC).

Spectroscopy

Photometry can be used to create SED plots that essentially resemble a sort of “low resolution” spectrum, using data from multiple instruments. An SED is the observed energy density (proportional to brightness) as a function of wavelength. A BB function is the theoretical description of the emission from an object that is thermally heated. Stars can be approximated as blackbodies; a pair of stars (or a star plus a dust ring) can be approximated as the sum of two blackbodies. SEDs can be fit by BBs, but all SEDs are not BBs and the terms SED and BB are not interchangeable. Data such as composition, rotation rate, motion relative to Earth etc. cannot be determined from an SED. These parameters require spectroscopy, which is the process of dispersing light into individual wavelengths (similar to using a prism to see a rainbow from the Sun or a lightbulb). Spectrographs attached to CCDs record counts of intensity (brightness) as a function of wavelength to produce a spectrum. A star’s actual spectrum reveals the differences between a true blackbody and the star -- it is much "messier" than a standard BB curve. “Dips” or absorption features are present as the chemicals composing the outer layers of a star absorb light at specific wavelengths (related to their atomic structure). These absorption features thus reveal composition as well as temperature (since at different temperatures, different elements are ionized, which affects the energies absorbed by that electrons of atoms in the star). The widths of these features can indicate rotation rate; the side of the star moving away from us is redshifted and the side of the star moving towards us is blueshifted, broadening the lines. Each element has a specific spectral pattern corresponding to specific wavelengths; if the entire pattern is shifted to bluer wavelengths, the object is moving towards us (blue-shifted), whereas if the spectral

pattern is red-shifted, it is moving away. While spectra are needed to determine data such as composition, motion of the target, age etc., an SED using photometry is enough to determine whether a target's emission profile resembles what is expected for a stand-alone star or if there is an excess of emission in the IR portion of the spectrum.

Finding the IR Excess

By plotting SEDs and comparing to a model (expected) curve based on parameters such as temperature, a large excess can be determined visually. Smaller amounts of dust create small IR excesses however, which are more difficult to identify. While larger IR excesses exceed any uncertainties, for smaller excesses, uncertainties in calibration along with measurement errors need to be accounted for, as do intrinsic stellar variations. To identify smaller IR excesses, a comparison of a short IR wavelength to the longest IR wavelength detection available is required. The relatively short wavelength samples the photosphere alone, without dust, and the long wavelength includes emission from the star and the dust. By comparing the emission expected from the star alone to the measured emission, any excess emission from the dust can be calculated. When examining WISE data, for example, by comparing the 3.4 and 22 micron bands, the presence of an IR excess can be determined. A commonly-used equation to determine the significance of any IR excess is:

$$\chi_{22} = \frac{([3.4]-[22])_{observed}-([3.4]-[22])_{predicted}}{\sigma([3.4]-[22])},$$

where χ is the significance of the excess, the values in brackets are the measurement of the brightness in that band (in microns), measured in magnitudes. Note that sigma is the

net uncertainty of those measurements. For a dust-free star, the expected photospheric color is [3.4]-[22]=0. By comparing the observed and predicted colors, taking into account the uncertainties on the measurement, we can assess whether there is a significant excess. A χ value ≥ 3 indicates the star has significant IR excess. If only one pair of measurements is available, only one χ can be calculated. If multiple measurements/bands are available, then a χ_{best} can be determined, taking into account measurements at other bands (Rebull et al. 2015; Mizusawa et al. 2012 and references therein).

Spatial Resolution

One of the challenges regarding detection of apparent IR excesses is that the IR excess may not come from dust around the WD, but instead a stellar companion or a BD or even a background/foreground object unfortunately superimposed on the target object. In order to resolve the WD plus a companion, one needs high spatial resolution observations. Resolution is how well an instrument can resolve two or more objects as individual targets. A classic example is "unmasking the face on Mars," in which Viking 1 recorded a feature known as Cydonia that seemed to resemble a face. Later missions showed that this was merely an illusion due to resolution (Figure 7). In the context of the present work, two sources that are close together on the sky (in projected distance, not necessarily physical, true distance) may not be separated into two distinct objects in the image. Lower resolution data may blur together a WD and neighboring target (such as a BD), making them seem like a single object when in fact there are multiple objects.

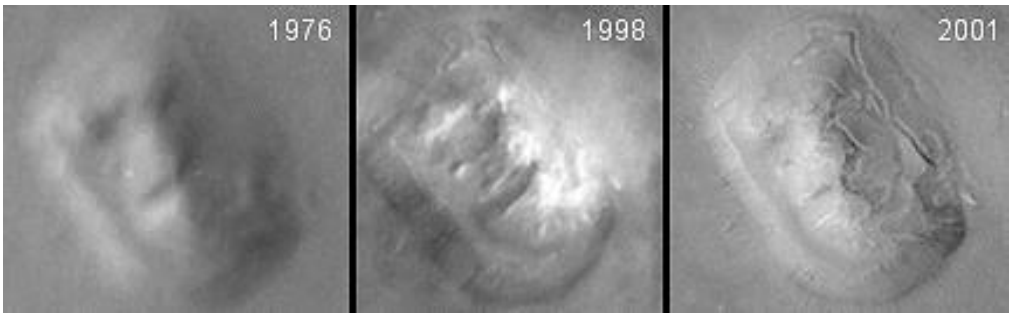


Figure 7. "The Face on Mars." The 1976 image is from Viking 1, the 1998 and 2001 images were taken by Mars Global Surveyor (MGS) (the latter from a high resolution camera). Low resolution of Viking 1 instruments made it difficult to discern clear details that MGS was able to resolve more easily. Credit: NASA. https://science.nasa.gov/science-news/science-at-nasa/2001/ast24may_1

Some instruments have better spatial resolutions than others; on the same telescope, some bandpasses yield better spatial resolution, e.g. the W1 bandpass of WISE has better spatial resolution than the W4 bandpass. The resolution limit is given by $1.22 \times \frac{\lambda}{D}$, where λ is the wavelength of light and D is the diameter of the telescope (with both wavelength and diameter in the same length units. Thus, within WISE, because the telescope mirror diameter does not change across bandpasses, but the wavelength does, the W1 (3.4 micron) images have higher spatial resolution than the W4 (22 micron) images; the spatial resolution at W1 is ~6.1 arsec, and at W4 it is ~12 arcsec.

FourStar data are higher resolution than WISE data, thus useful in determining if neighboring or background targets might have been combined in the WISE source, leading to an apparent excess that in fact is not truly arising from the target of interest. Comparing the WISE and FourStar data is the easiest way of determining whether or not the IR excess is due to an apparent (projected) companion or not; however, companions can be located closer to the target star than can be resolved with FourStar.

If the higher spatial resolution observations with FourStar do not reveal a companion, modeling is an additional way to check to see if the apparent IR excess comes from a companion. Debes et al. (2012) determined that SDSS J030308.35+005443.7 consists of a He WD and a MS red dwarf star (M4.5 dwarf) by fitting model curves of M dwarfs and WDs to the photometry (Figure 8). They discovered an unexplained excess still remained present after fitting the WD plus M4.5 dwarf, and once a curve representing a circumbinary disk (a disk around both targets) was added, the sum of the model curves matched the SED from the data. The source of the disk is thought to be either destruction of planetary bodies from the combined gravitational forces or dust from the M dwarf's winds.

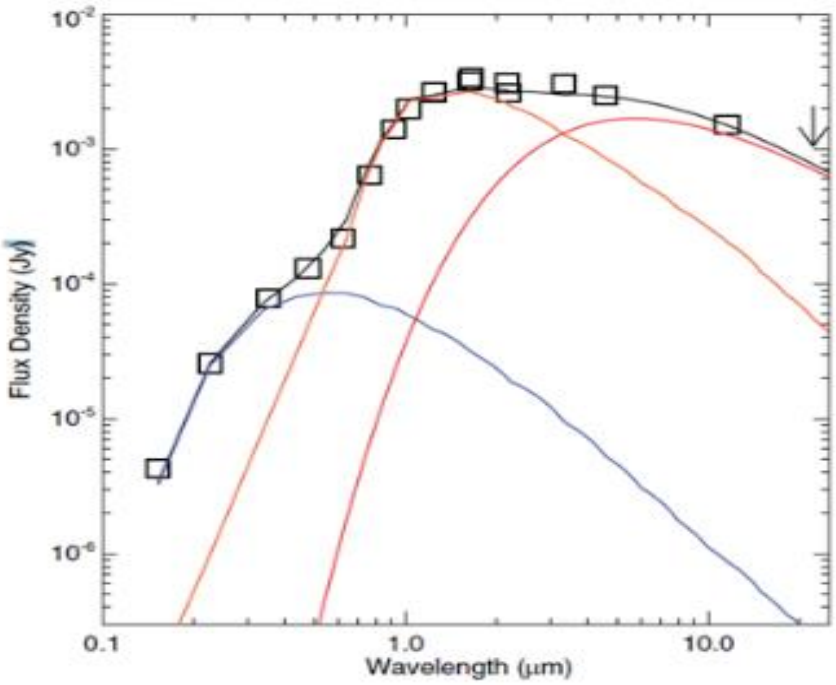


Figure 8. Plot of flux density vs. wavelength for SDSS J03030835+005443.7 by Debes et al. (2012, p. 19). The black line is the combination of the WD (blue line), stellar companion (orange line), and circumbinary dust disk (red line).

Proper Motion

Proper motion is the motion of a target compared with background stars (angular velocity). Targets with larger proper motions tend to be closer to our Solar System. Since WDs are faint, it makes sense that most known WDs are closer and thus have significant proper motions. For objects that have high proper motions (HPM), observations taken from different surveys at different times will have the object at significantly different locations, which makes it challenging to find counterparts and can lead to source confusion in some surveys that is absent in others. One second of arc (arcsecond) is written as 1"; there are 3600" in a degree. A typical proper motion is 0.1"/year, the star with the largest known proper motion is Barnard's Star, with a proper motion of 10.25"/year (Saha, p. 416).

Overview of Approach

1. Assemble target list of objects using FourStar observation logs from two nights of observations: 07-23-2013 and 07-24-2013.
2. Look for additional information and counterparts in the SIMBAD database (Wenger et al., 2000). Obtain spectral types from literature, good coordinates, and identify which targets have significant proper motions.
3. Assemble data from 2MASS, UKIDSS, WISE, FourStar (if 2MASS or UKIDSS data are not available), DENIS, Spitzer, SDSS and PanSTARRS. Make sure targets with high proper motions are matched correctly across all these surveys. Convert all magnitudes to flux densities. Assemble SEDs for each object.

4. Use IDL programs from Dr. Stark to do basic CCD reductions. Attach WCS (coordinate system) to images with astrometry.net.
5. Write IDL programs to use aperture photometry routine (aper.pro) to perform photometry on the FourStar images and calibrate the photometry.
6. Examine FourStar data using the imaging software DS9 (Smithsonian Astronomical Observatory) and determine if there are potentially additional targets in the WISE beam that could account for an apparent IR excess; if another background object is present within a small (<6") angular separation, this is an example of potential source confusion.
7. Determine model SEDs using code provided by Dr. Debes, which is based on models created by Holberg & Bergeron (2006), Kowalski & Saumon (2006), Tremblay, Bergeron & Giannas (2011), and Bergeron et al. (2011). Look for whether there is a significant, measurable IR excess (compare to other data on that object and/or model).
8. Determine if a neighboring target is contributing to the excess—this is source confusion.
9. If the excess is not due to source confusion and extends short of the H band, the excess is likely due to an M dwarf or BD companion. If the excess is only present beyond 2 microns, this excess is either due to a dust disk or a cold brown dwarf.
10. For those that might have a small excess (based on the SED), use χ calculations to verify if a significant excess may be present.

DATA AND ANALYSIS

Assemble Target List

This study was originally motivated, at least in part, by the availability of FourStar data; consequently, the target list is inhomogeneous. The target list was originally assembled from a variety of sources. Twenty-one targets were initially determined to have a 10σ excess in at least one filter in the SDSS r band or longer, or a >3σ excess in the W1 band or longer by Debes et al. (2011) in the WIRED II survey. Another 18 were selected from the McCook & Sion White Dwarf Catalog (Hoard et al., 2013). Twenty-seven additional candidates came from other studies due to telescope time available during the time the FourStar observations were made, including a SuperCOSMOS Sky Survey study conducted by Rowell & Hambly (2011) and a table of known dusty WDs by Barber (2014). To proceed, we needed to obtain precise coordinates for these objects. Coordinates to better than 1" were obtained using SIMBAD, FinderChart and FourStar images (see Appendix A).

Counterparts, Spectral Types, and Proper Motions

The SIMBAD database was used as a starting point to determine counterparts as well as spectral types of WDs. Many objects have multiple catalog names, for example SDSS J005438.84-095219.7 has 10 identifiers listed in the database. SIMBAD can often be inaccurate, so references where available were used to verify spectral classifications. More than 20% of the sample did not have data available in SIMBAD. Of the 66 targets, 39% have high proper motions, and 18% of the sample are metal-rich (Figure 9).

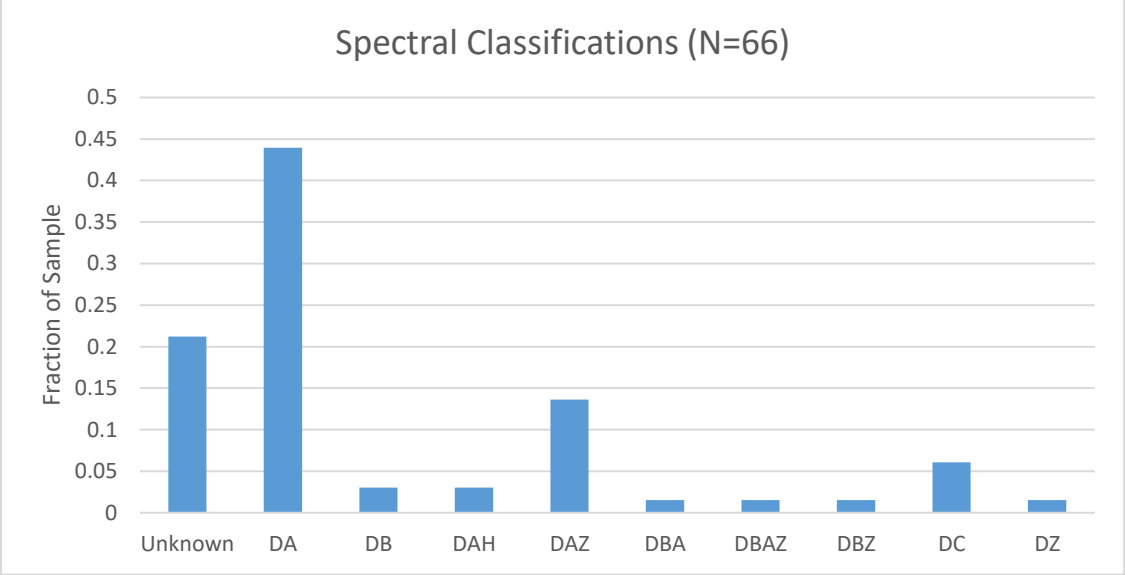


Figure 9. Distribution of spectral classifications. Targets with classifications ending in "Z" are metal-rich WDs.

Archival Data

There is a lot of astronomy data available for free online. Many of these archives are being used in high school classrooms around the world; see e.g. Fitzgerald et al. (2014). We took the target list as assembled above and looked for counterparts in a wide variety of surveys. The data used in this study are primarily IR data, although SDSS data and Pan-STARRS data also include optical and near UV bands to complete the shorter wavelength regions of the SED. See Table 1 for a list of the surveys, wavelengths, and spatial resolutions, and Figure 10 regarding the percentage of the sample with data from each survey.

Table 1
Instrument/Survey Data

Instrument/Survey	Band-passes	Resolution
Sloan Digital Sky Survey (SDSS) SDSS (2015).	u: 0.3551 μm g: 0.4686 μm r: 0.6166 μm i: 0.7480 μm z: 0.8932 μm	1.3”/pixel
Panoramic Survey Telescope and Rapid Response System (PanSTARRS) Kaiser, N. et al. (2002). Rest, A. & Scolnic, D. (2017).	g: 0.4866 r: 0.6215 i: 0.7545 z: 0.8679 y: 0.9633	0.258”/pixel
Deep Near Infrared Survey of the Southern Sky (DENIS) Deul, E. (1992).	i: 0.778 μm J: 1.221 μm K: 2.144 μm	1”/pixel in I; 3” in J and K
The UKIRT (UK Infrared Telescope) Deep Sky Survey (UKIDSS) Dye et al. (2006)	J: 1.2483 H: 1.6313 K: 2.2010	0.4”/pixel
The Two Micron All Sky Survey (2MASS) Skrutskie et al. (2006); Cohen et al. (2003)	J: 1.235 μm H: 1.662 μm K_s: 2.159 μm	2”/pixel
FourStar Infrared Telescope Persson et al. (2013) and this work.	J: 1.25 μm H: 1.65 μm K_s: 2.15 μm	0.159”/pixel
Spitzer Space Telescope Werner et al. (2004). SEIP: http://irsa.ipac.caltech.edu/data/SPITZER/Enhanced/SEIP/overview.html	I1: 3.6 μm I2: 4.5 μm I3: 5.8 μm I4: 8.0 μm M1: 24.0 μm	1.2”/pixel for IRAC bands; 6”/pixel for MIPS 24 micron
Wide-field Infrared Survey Explorer (WISE) Wright, E. L. et al. (2010).	W1: 3.4 μm W2: 4.6 μm W3: 12 μm W4: 22 μm	6.1” 6.4” 6.5” 12.0”

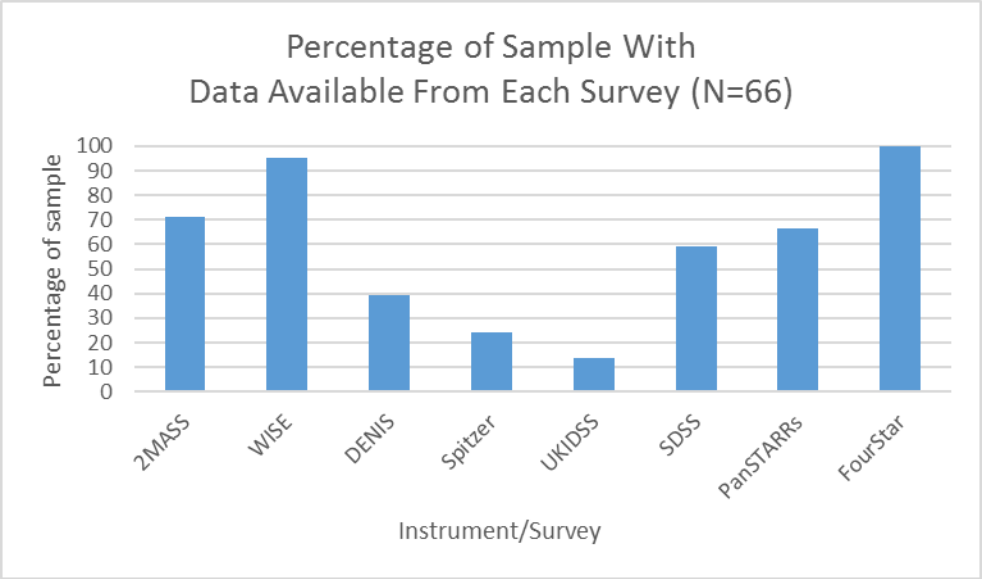


Figure 10. Percentage of Sample with Data Available from Each Survey (N=66).

Most of these targets had counterparts in these surveys within 1 to 2 arcsec. Finding counterparts to those WDs with HPM was complicated, since the surveys listed in Table 1 were obtained over many years. Each target was examined by hand using IRSA's FinderChart tool (IRSA, 2016) to inspect images from SDSS, 2MASS, and WISE, and overlay catalogs from these and other surveys as obtained from IRSA's catalog search tool. WISE images and catalogs were compared in FinderChart and using DS9 to be sure that the target was truly detected in the W3 and W4 images, as explained in Rebull et al. (2015).

We then assembled SEDs to make sure the targets were matched correctly across wavelengths and surveys and to check for IR excesses (see "Interpretations and Conclusions" for sample SEDs and Appendix B for all SEDs). These SEDs should be smoothly varying; an obvious discontinuity or offset of data points from one survey with respect to the rest of the surveys indicates that the source is probably not properly

matched in that survey. For each case where there was a problem with the initial SED, the cross-matching for that source was inspected and removed or corrected. Several sources required manual overrides in the programming to address source confusion in WISE, particularly HPM stars.

New Data (FourStar)

The new data presented here come from FourStar, an instrument that takes images in the near-IR (J, H, K_s bands) from the Magellan telescopes at Las Campanas, Chile as part of Carnegie Observatories. FourStar data were obtained in July of 2013 by Dr. Debes and Dr. Stark of the Space Telescope Science Institute. Data were reduced via a pipeline provided by Dr. Stark and run by Dr. Rebull. This pipeline calibrates pixel-by-pixel responses (known as flat-fielding), and shifts and adds the images taken as part of the observing sequence (which are groups of five images taken at slightly different positions). The images at this point are neither flux-calibrated (converting the native units of the image as it comes off the camera – counts – into units that tie the brightness of these sources to those elsewhere in the sky) nor calibrated for position on the sky (correspondence between pixels on the image to RA and Dec on the sky). Both of those steps are necessary before proceeding further.

To attach the coordinates to the image, astrometry.net (Lang et al. 2010) was used to attach world coordinate system (WCS) keywords to each FITS image header. This service detects point sources in the images and compares them to its library of star positions all over the sky. In this fashion, it figures out the coordinates of all the bright

sources in the images. It then includes this coordinate information into the image itself (the FITS header), and then subsequent software (like IDL or ds9) can translate between pixels and position on the sky.

FourStar Photometry

In order to flux calibrate each image, we relied on 2MASS to bootstrap our calibration. 2MASS observed the whole sky in the same bands that we are using in FourStar, J, H, and Ks. For each image, in each band, we followed these steps:

- For the region in the sky covered by the image, retrieve 2MASS data.
- For each object in the region, take its 2MASS position, go to its corresponding RA/Dec in the FourStar image and do aperture photometry in the FourStar image at that location (using the IDL Astronomy Library code aper.pro).
- Compare the photometry obtained in the FourStar data with those from 2MASS in the same band of the same star.
- Flux calibrate the FourStar data by deriving the offset between the 2MASS calibrated magnitudes and the FourStar measured magnitudes for that image.
- Measure the brightness of the target star in the FourStar image, and use the derived calibration to obtain the measured brightness in calibrated magnitudes for the FourStar image.

In practice, this was more difficult than anticipated. Astrometry.net failed to attach coordinates at all to some images, and had to be substantially helped along (telling

it a guess at the position and image size) before it would put positions on most of the images. The astrometry in some cases we suspect is still not very good, at least not good enough for this specific approach. Some fields did not have very many sufficiently bright stars that were also found in 2MASS. As result of these issues, we decided to focus on obtaining photometry from the FourStar data for those targets still lacking NIR data from UKIDSS or 2MASS. The measured FourStar photometry appears in Table 2. Errors as returned from the aper.pro routine are statistical and not systematic, and thus underestimated. We estimated errors from the scatter in the most well-populated plot comparing 2MASS and FourStar. These FourStar data were then added to the SEDs (Appendix B).

Table 2
FourStar Photometry

Target	J Mag	Jmerr	H Mag	Hmerr	K Mag	Kmerr
011616.94-094347.9	…	…	…	…	19.099	0.579
144847.79+145645.7	17.618	0.012	17.516	0.012	17.691	0.041
153149.04+025705.0	18.613	0.023	18.332	0.036	18.262	0.034
160153.23+273547.1	16.644	0.026	…	…	16.926	0.012
160715.8+1314312.3	17.515	0.049	…	…	17.47	0.049
160839.52+172336.9	17.499	0.058	17.505	0.058	17.977	0.141
161717.04+162022.3	17.15	0.07	17.36	0.065	…	…
231725.28-084032.9	17.42	0.025	17.264	0.03	17.196	0.03
J2209+1222	17.315	0.028	17.3	0.037	…	…

Source Confusion

As mentioned earlier, many targets were chosen due to the presence of an IR excess in WISE. The presence of an IR excess could either be due to a BD companion, a nearby background or foreground star (meaning a target near that location that is not necessarily physically close to the target—just appears close in projection on the sky from our perspective), or a disk. FourStar data are higher spatial resolution than WISE data, so one of the goals of this study was to identify whether there were bright IR sources near to the primary target that could contribute to the WISE detection. In Rebull, et al. (2015), a similar issue was observed with IRAS data vs. WISE data, in which many objects that seemed to have an IR excess in fact did not; the "false positive" resulted from source confusion due to spatial resolution. In order to identify instances in which source confusion indicated a false IR excess, the FourStar and WISE data were loaded into ds9 as a multi-color image, with the blue plane (B) as WISE 1 and the red plane (R) as FourStar J. By overlapping these images, it is easy to see when several targets as identified by FourStar are confused as a single target by WISE. If there is an IR bright source within the WISE beam, then the IR excess measured by WISE could be due to that source and not the WD (see "Interpretation and Conclusions" for examples).

Model Curves

Models were calculated by J. Debes using known temperatures of the WD targets from the literature, a single log g = 8.0 typical for hydrogen WDs, and known data on age and distance (Appendix C) based on parameters provided by Holberg & Bergeron (2006), Kowalski & Saumon (2006), Tremblay et al. (2011), and Bergeron et al. (2011).

IR Excess Determination

For large IR excesses, simply comparing by eye the lines in the SED (from the model and/or the Rayleigh-Jeans line) is enough to identify those WDs with excesses. To quantify the excess, or for those WDs with more subtle excesses, the significance of the IR excess must be calculated. χ values were calculated comparing:

- K_s to WISE 12 micron
- WISE 3.4 micron to WISE 12 micron
- K_s to Spitzer 5.8 micron
- Spitzer 3.6 micron to Spitzer 5.8 micron

For SEDs in which the IR excess is present at <2 microns, these were identified as WD+BD candidates. SEDs with IR excesses beginning around 2 microns (K_s) were identified as disk candidates.

INTERPRETATION AND CONCLUSIONS

Each target falls into one of the following categories (Figure 11):

- IR excess, but likely due to source confusion detected in images.
- Real IR excess, but based on where the excess begins (around J or H band), a BD companion is the likely source of the IR excess.
- Real IR excess, no source confusion as far as we can tell, so thus a disk candidate.
- No IR excess, no source confusion; WD data fits model curve.
- Determined not to be WD stars

To further characterize the nature of an excess and whether a BD or a disk (or combination of the two) requires additional modeling. For now, characterizations are predicted based on the level of IR excess and where in the SED the IR excess becomes present (exceeds the model).

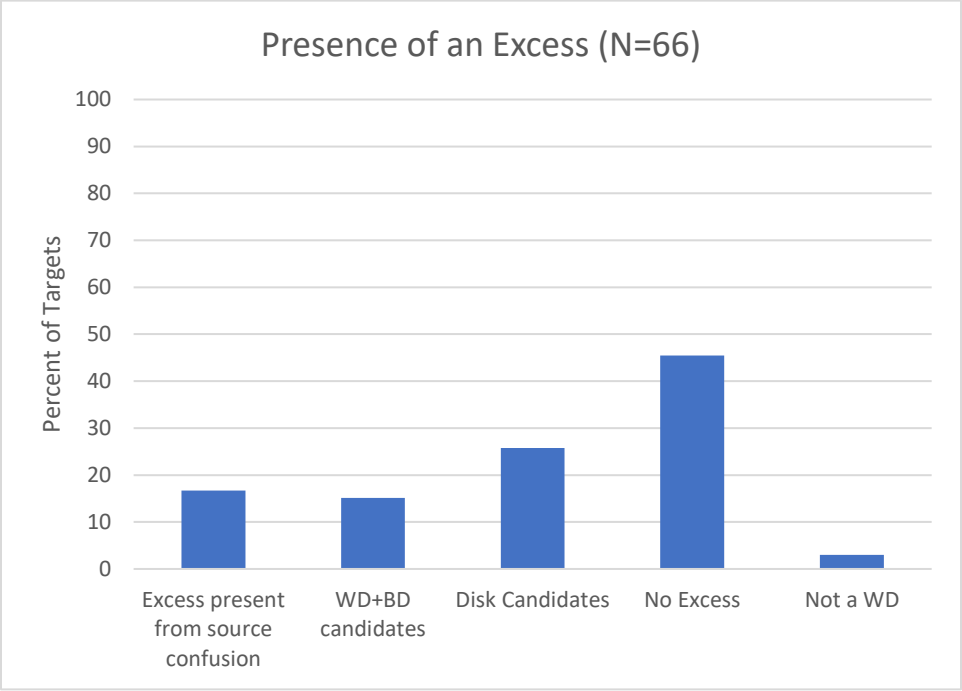


Figure 11. Presence of an Excess. About a quarter (26%) of the sample appear to have an excess not attributed to a BD companion or entirely to source confusion, which is relatively consistent with statistical studies outlined earlier in "Conceptual Framework." Three targets are identified as having a contributing excess from source confusion but are still thought to have disk; these are all metal-rich. One target is categorized as both a WD+BD candidate and as having an excess from source confusion.

Most excesses were large enough that they could be identified visually based on SEDs (Appendix B). Note that WISE limits in SED images (as discussed in "methodology") are indicated by "↓'s". Three additional candidates' excesses were identified via χ calculations (Table 3). One target— J142439.3+091716 was confirmed to be a WD+BD companion, so it is expected the excess is a result of the companion, which was resolved and identified using the imaging software DS9 and the catalog features available in DS9.

Table 3
χ Calculations (Small Excesses).

Target	$\chi_{Ks-[12]}$	$\chi_{[3.4]-[12]}$	$\chi_{Ks-[5.8]}$	$\chi_{[3.6]-[5.8]}$	Conclusion
FS-34	4.712	4.883			Excess candidate
J142439.3+091716			2.808	2.837	GD 165, known WD+BD (L4) binary (Steele et al., 2007; Zuckerman & Becklin, 1992).
WD0029-031				3.526	Excess candidate

IR Excess Due to Source Confusion

Eleven targets have IR excesses resulting from source confusion (Table 4); 3 however are still suspected of having a disk and 1 may have a BD companion. Three of the targets were also identified as "blended" by Barber et al. (2014).

The SED of target 153149.04+025705.0 shows a very large excess in WISE (Figure 12). FourStar data show two objects within a region of 1.77" (Figure 13). It seems WISE is interpreting these two objects as being a single target. The identification of the neighboring target is unknown. Given that these targets are resolved in FourStar, and that the H and K_s data are above the model, it is possible there is an additional source of excess (e.g a BD); the WISE excess however is too large to be from this source entirely (it should follow the same trend as the FourStar data). Barber et al. (2014) identified this as a blended source.

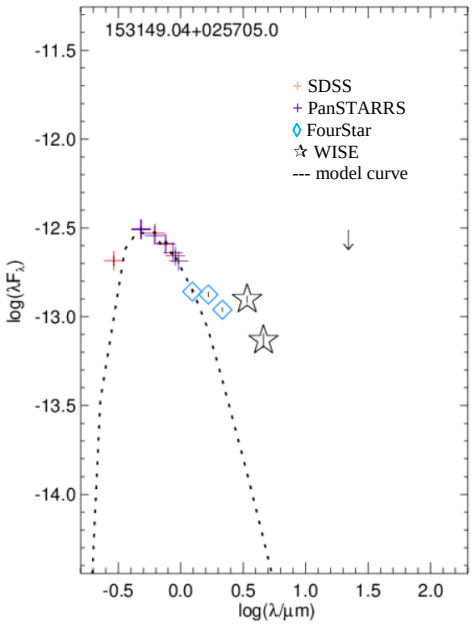


Figure 12. SED for 153149.04+025705.0. The level of excess in WISE is too great to be the result of a BD or disk, and is likely due to source confusion. Note the W4 value is a limit, denoted by "↓."

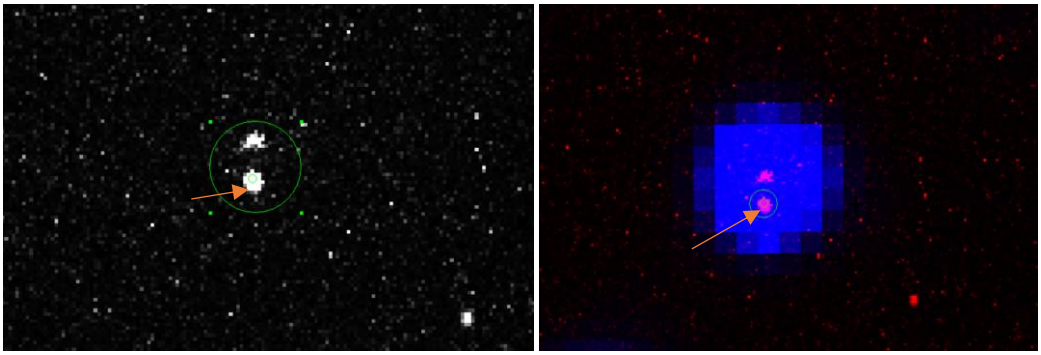


Figure 13. The image on the left is FourStar J data of 153149.04+025705.0.; the image on the right shows an RB image of the FourStar J band data (red) and WISE W1 data (blue); where WISE sees one target, FourStar sees two. We conclude that the IR excess in WISE (Figure 12) is the result of source confusion.

WD1929+012 is GALEX J1931+0117, and was discussed in "Conceptual Framework" as a known dusty WD based on the WIRED I Survey (Debes et al., 2011). The WISE portion of the SED however is likely contaminated (Figure 14). FourStar indicates at least two blended sources; 2MASS and WISE see them as a single target

(Figure 15). The target is still suspected of being dusty, as Debes et al. (2011), Vennes, Kawka and Nemeth (2011) and Melis et al. (2011) still found an excess after accounting for the presence of the blended source. The WISE portion of the SED does not accurately characterize the excess.

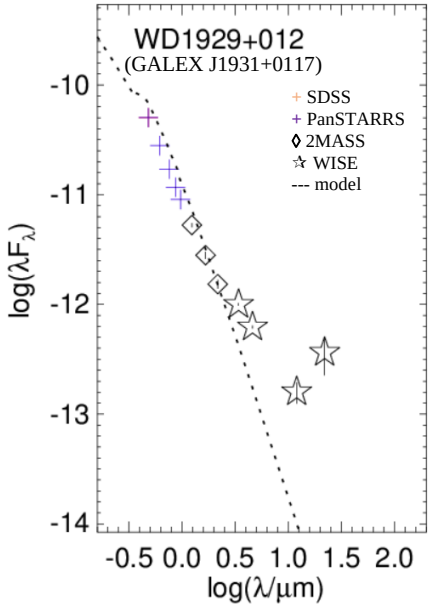


Figure 14. SED of WD1929+012/ GALEX J1931). Some of the apparent IR excess here might be source confusion, but literature says at least a portion of the excess is due to a disk.

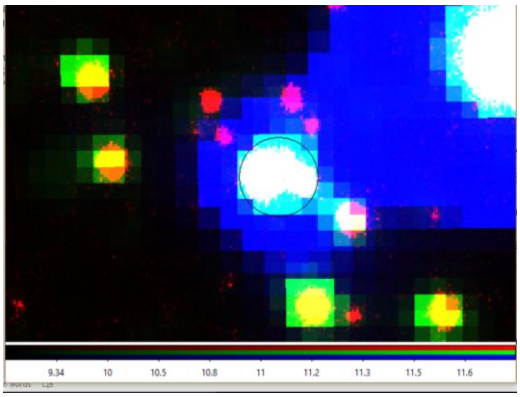


Figure 15. RGB image of WD1929+012/GALEX J1931. Red is FourStar J, green is 2MASS J, and blue is WISE 1. In a 2.55" region (black circle) there are at least two objects that are blending.

Another example of potential source confusion is WD 0106-328 (Figure 16). Identified by Farihi et al. (2010) as a dusty WD, the WISE data of the SED (Figure 17) differs from the rest of the data; as seen in figure 15, the WISE points at W1 and W2 are above the IRAC points at I1 and I2. Both I1 and W1 are very similar wavelengths (as are I2 and W2), but Spitzer/IRAC has higher spatial resolution and thus those measurements are likely a more accurate assessment of the brightness of this target. Spitzer indicates an excess (χ of [3.6]-[5.8] = 4.028 and χ of [3.6] – [8] = 5.577), but the excess in WISE does not align with the rest of the data, due likely to source confusion. This is probably a legitimate dusty WD, but the WISE portion of the SED does not characterize the excess accurately.

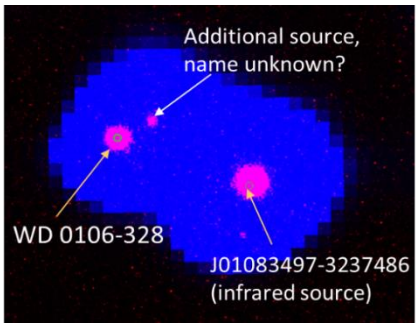


Figure 16. Photometric RB image of WISE 1 (blue) and FourStar J (red) for WD0106-328.

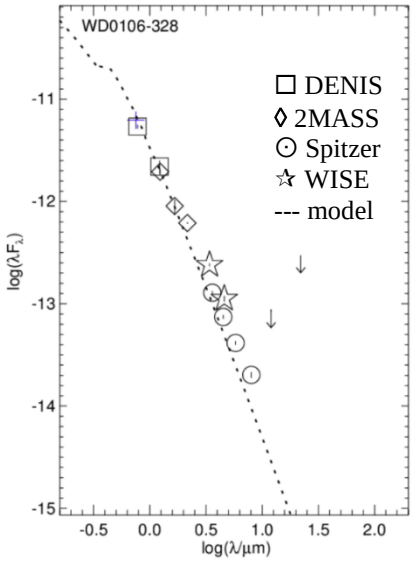


Figure 17. SED of WD0106-328,

Table 4
IR Excess Due to Source Confusion

Target	Spectral class	Additional notes
164216.62+225627.8	DA	Nearby resolved object, 2MASS and WISE see as single target
J012500.7+181140	?	Neighboring object resolved, WISE sees as one target
011616.94-094347.9	DA	Nearby target, blend at edges in FourStar
J011932.1-141527	DA	Neighboring target, WISE sees as one
155359.87+082131.3	DA	Blended; Barber et al. (2014) identified as confused as well.
153149.04+025705.0	DAH	Blended; Barber et al. (2014) identified as confused as well. WD+BD?
J224626.38-005909.2	DA	Blended; Barber et al. (2014) identified as confused as well.
WD0106-328	DAZ	Nearby target leading to source confusion in WISE; excess beginning at 2 microns in 2MASS K and Spitzer still expected to be from a disk.
WD1919+145	DA	Nearby target are visible in FourStar, blends at edges however, thus likely source confusion in WISE. The remaining data follow the model.
WD1929+012 WD1929+011 GALEX J193156.8+011745	DAZ	Considered known dusty; target blends with neighboring objects, excess likely is a combination of a disk and source confusion.
WD1456+298	DAZ	Definite excess beyond 3 microns, more prevalent in WISE than in Spitzer; likely has a disk, with source confusion adding to the excess in WISE

WD+BD Candidates

Ten targets are identified as WD+BD candidates due to the fact there is an IR excess present in the SED which begins around the J or H band. Seven of these are new WD+BD candidates (Table 5). Further modeling is needed to determine if a disk is also contributing to the IR excess. A few of these companions have been resolved in FourStar, but most have not.

Table 5
WD+BD Candidates

Target name	Spectral class of WD	Known WD+BD?	Companion resolved?
012532.02+135403.6	DC	No	No
013532.97+144555.9	DA	DA+dL5 (Steele et al., 2011)	No
144847.79+145645.7	DA	No	Faint source within 3”
160153.23+273547.1	DA	No	Faint source within 3”
160839.52+172336.9	DA	No	No
222030.69-004107.3	DA	DA+dL8 (Steele et al., 2011)	No
231725.28-084032.9	DA	No	No
J000747.6+195125	?	No	No
J142439.3+091716	DA	This is GD165, known WD+BD (Zuckerman & Becklin, 1992).	Yes (using DS9 as well as FinderChart)
153149.04+025705.0	DAH	No	No; excess in WISE influenced by source confusion, but excess in H and K may indicate a BD companion.

Target 231725.28-084032.9 was initially flagged as containing an "indeterminate excess" by Debes et al. (2011). The RB image (Figure 18) is elongated. There seems to be an excess in FourStar and WISE portions of the SED (Figure 19). Wang et al. (2014) also determined the target to have an IR excess, and also noted that the stellar properties differ from WDs known to have debris disks. The only other option is an unresolved companion contributing to the excess; this is likely a BD just based on where the excess begins (FourStar H).

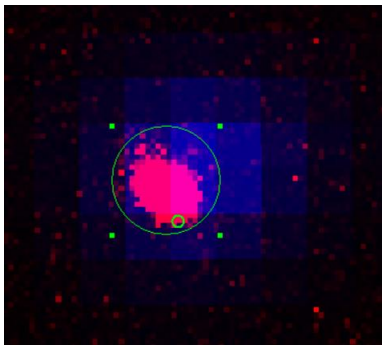


Figure 18. RB image of 231725.28-084032.9. Blue is WISE, red is FourStar J data. The target is semi elongated, there are no known sources of confusion or visible companions.

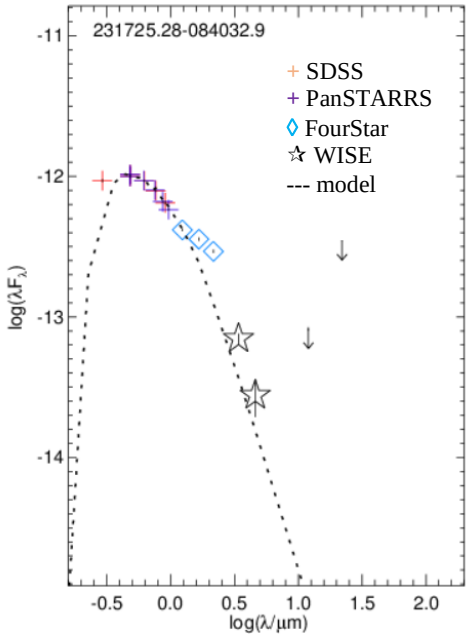


Figure 19. SED of 231725.28-084032.9. An excess begins around the H and K band and continues into W1 and W2. This indicates the likely presence of an unresolved BD companion. Note that W3 and W4 are limits (indicated by ↓).

Disk Candidates

Seventeen targets are identified as disk candidates (Table 6), 7 of which are newly confirmed in this work. Eleven of the targets are known to be metal-rich (DAZ, DBZ or DBAZ). The remaining candidates are primarily flagged as DA, but are lesser known and studied, so further spectral analysis may be needed.

WD 2115-560 was identified by von Hippel et al. (2007) as a dusty DAZ WD using Spitzer IRAC data. This target has an obvious excess above the model beginning at 3 μm (Figure 20), and no nearby sources contributing to source confusion are seen (Figure 21).

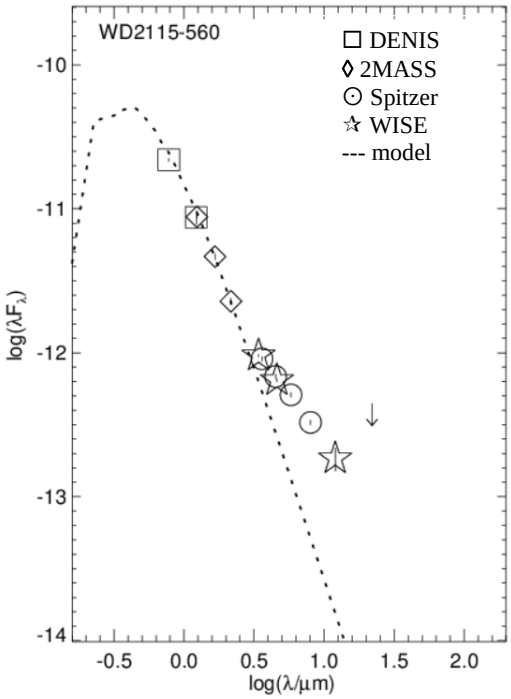


Figure 20. SED of WD 2115-560, a known dusty WD. The IR excess begins at 3 microns (WISE and Spitzer).

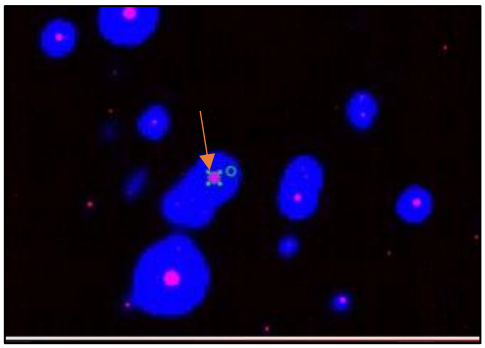


Figure 21. RB image of WD2115-560, red denotes FourStar J data, blue is WISE W1 data. Aside from the very faint background, there are no apparent sources surrounding the target of interest.

Table 6
Disk Candidates

Target	Spectral Class	Known Dusty?	Additional Notes
WD2326+049	DAZ	Yes	Nearby source, but WISE and Spitzer agree
222416.84-161534.7	DAZ	Yes (a.k.a. WD 2221-165)	Excess in Spitzer
WD1456+298	DAZ	Yes	Some source confusion in WISE
154729.96+065909.5	DZ	No (NEW)	Excess in WISE, no source confusion
000410.42-034008.5	DA	No (NEW)	Beginning in 2MASS K
005438.84-095219.7	DA	No (NEW)	Excess in WISE, no source confusion
J2209+1222	DBZ	Yes	Begins at H band, so possible companion instead of disk
WD0106-328	DAZ	Yes	Some source confusion in WISE
WD0110-565	DBAZ	Yes	Excess beginning in 2MASS K
WD2115-560	DAZ	Yes	Clear Excess in WISE and Spitzer
J1557+0916	DAZ	Yes	Excess beginning in UKIDSS K
160715.80+134312.3	DA	No (NEW)	Only in FourStar K
143406.75+150817.8	DA	No (NEW)	Excess in H and WISE (but not K), suspect H band value has an error
161717.04+162022.3	DA (?)	Yes (Wilson et al. 2014).	Begins at H band so might also be BD candidate
WD0029-031	DA	No (NEW)	Presence of excess determined using χ values (table 3)
FS-34	DA	No (NEW)	Presence of excess determined using χ values (table 3)
WD1929+012 WD1929+011 GALEX J193156.8+011745	DAZ	Considered known dusty; target blends with neighboring objects, excess likely is a combination of a disk and source confusion.	WD1929+012 WD1929+011 GALEX J193156.8+011745

Target 161717.04+162022.3 has only been recently identified as a dusty candidate, but based on time-series spectroscopy (as opposed to the photometric methods used here). According to Wilson et al. (2014), time series spectroscopy obtained from 2006–2014 revealed strong Ca II lines in 2008, thought to have resulted from the impact of a planetesimal or material from a "debris tail" onto a disk that then accreted onto the WD (p. 1883). Radiative levitation would not be a possible internal mechanism as too high of a temperature is required for Ca emission lines to be produced (lighter elements such as Si still require large temperatures, as discussed in "Conceptual Framework"). The target's SED (Figure 22) supports that this is a dusty candidate, as both FourStar and WISE data are above the model and thus indicate an excess.

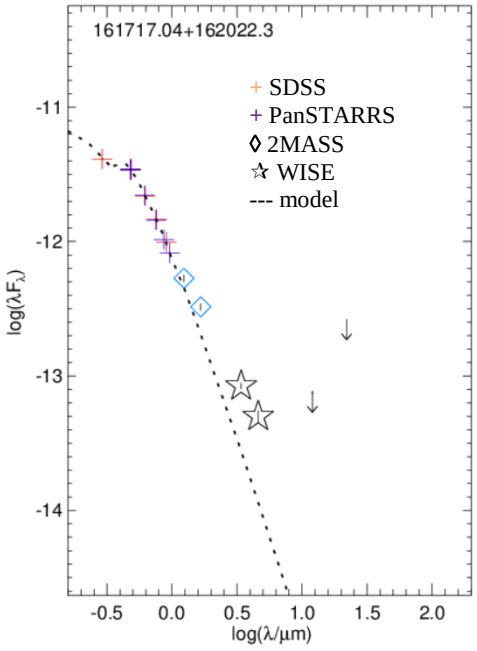


Figure 22. SED of 161717.04+162022.3. An excess is clear in WISE and in FourStar which are above the model. There are no visible sources of confusion in the imaging.

No IR Excess, No Confusion

GD 153 is an example of a target whose data fits the model for a non-dusty WD very well (Figure 23). GD 153 as well as FS-1 are both known, dust-free WDs, included as calibration stars. Since we did not identify IR excesses in these stars, we therefore have confidence that our approach is working in general. Twenty-nine additional targets likewise align with the model curve, indicating the absence of an excess.

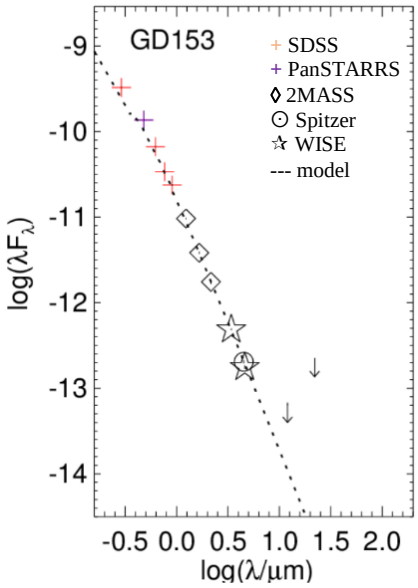


Figure 23. SED for GD 153; the data clearly follows the model.

Target PG 1457-086 is a metal-rich DAZ WD. Farihi, Jura & Zuckerman (2009) identified it as having an excess over 3σ at both 3.6 and 4.5 μm, but that the 2MASS photometry has large errors in H and K_s. Based on the Spitzer data and its metal-rich nature, Farihi et al. (2009) classified PG 1457-086 as dusty. The SED (Figure 24) however only shows a significant excess in 2MASS K_s. χ values are small (1.324 for $\chi_{Ks-[5.8]}$, and 0.7351 for $\chi_{[3.6]-[8]}$), thus in this work this target is not classified as a dusty candidate.

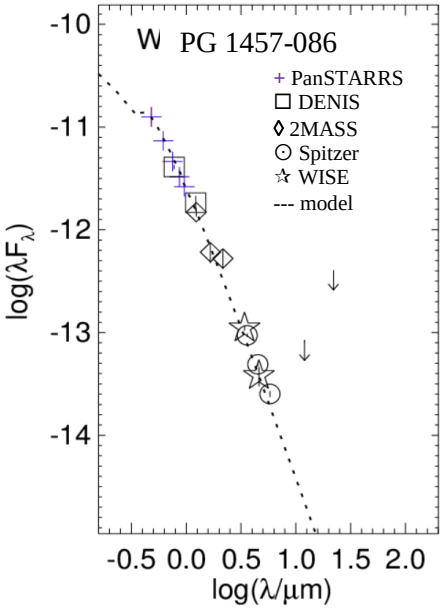


Figure 24. SED of PG 1457-086; there is a potential slight excess in Spitzer (though small); only 2MASS K_s is dramatically above the model.

Not a WD

Two targets, 172920.9-085409.4 and J231222.7+161555, were determined not to be WD stars after all, but likely red M dwarfs instead (small, red, main-sequence stars). This is based on the fit to the SEDs and the temperature that results from the fit. J231222.7+161555 is a HPM star known as LSPM J2312+1615 (Lepine & Shara, 2005); 172920.9-085409.4 is a HPM star known as LP 687-39 (Luyten & Hughes, 1980). Not much else is known about these targets.

Summary

The goal of this study was to determine, of a sample 66 targets, how many have IR excesses, and the potential sources of excess. Such studies provide insight into the fates of planets following the deaths of their stars. Seventeen targets are classified as disk candidates, 10 of which are known to be metal-rich; 7 of these 16 targets are newly identified here as disk candidates. Three of these targets have excesses in WISE that are at least partially influenced by source confusion. Ten WD+BD candidates were identified, 7 of which are newly identified, 1 of which also likely has a contribution from source confusion. The SEDs of 11 targets are impacted by source confusion from nearby targets in WISE bands, including known dusty WDs WD 1456+298, WD 0106-328 and WD 1929+012/GALEX 1931+0117. WD 1456+298 and WD 0106-328 show less of an excess in Spitzer, which has better resolution than WISE. GALEX 1931+0117 remains identified as a dusty WD as other studies accounted for this source confusion and still found indication of a disk. All three of these are metal-rich. We agree that 3 targets are

blended sources as identified by Barber et al. (2014), although one may have a companion based on the excess present in FourStar H and K_s. The remainder of the sample follows expected models of non-dusty WD stars, including PG 1457-086, which in literature was identified as having a small excess; the χ values we found however are quite small, indicating an insignificant excess. Two targets were found to not be WDs after all.

VALUE

Scientific Value

- This is the first time all these data have been assembled together for these targets.
- New FourStar data was added to 9 targets not previously measured in J, H and K_s before.
- 34 targets were found to have excesses:
    - 17 are disk candidates, 7 of which are newly identified, 10 confirmed from literature
    - 10 are WD+BD candidates, 7 of which are newly identified, 3 confirmed from literature.
    - 7 targets have excesses attributed entirely to source confusion.
- 30 targets found to not have a significant excess, including PG 1457-086, identified previously as having a very mild excess.
- 2 targets are now known to not be WD stars.

To determine whether disk candidates as well as WD+BD candidates are properly identified, further modeling is needed (i.e. fitting a WD+BD model curve to the data of a

WD+BD candidate), as discussed in "Conceptual Framework" in relation to the WIRED papers (Debes et al. 2011; Debes et al. 2012). An additional next step includes improving upon some targets' models. Additionally, warm Spitzer data may be available in the Spitzer Heritage Archive, which will require doing more photometry. These steps will be completed prior to publication of this work in a scholarly journal.

Educational Value

- Lots of archives of data are available for free, and many archives have great tools (e.g. FinderChart). Photometry has already been done for most archival data, presenting authentic hands-on science opportunities for student research groups.
- While blackbody radiation may be covered in some physics and astronomy courses, SEDs are not taught; however, SEDs are an important component of astronomical research, and students can better understand how the "crazy cool findings" we hear about in the news are determined by studying SEDs.
- As a teacher, engaging in scientific research allows me to show students a more accurate concept of what the scientific research process looks like. Throughout the year, I have shared about my research progress, allowing students to gain a better understanding of the nature of science, e.g. that it is non-linear and does not follow a prescribed "scientific method." Some students interested in STEM careers do not realize how much writing is required or creative problem-solving is involved. By showing students research papers and posters, they know what a career in STEM might look like.

REFERENCES CITED

Barber, S. D., Patterson, A. J., Kilic, M., Leggett, S. K., Dufour, P., Bloom, Starr, D. L. (2012). *The Frequency of Debris Disks at White Dwarfs*. ApJ, 760(1):26-37. http://iopscience.iop.org/article/10.1088/0004-637X/760/1/26/pdf

Barber, S. D., Kilic, M., Brown, W. R., & Gianninas, A. (2014). Dusty WDs in the WISE All Sky Survey. ApJ, 786:77-82. http://iopscience.iop.org/article/10.1088/0004-637X/786/2/77/pdf http://www.nhn.ou.edu/~barber/Research.html

Barber, S. D. *Dusty White Dwarfs.* (2014), https://www.nhn.ou.edu/~barber/Publications.html. Accessed 07 June 2017.

Bass, S. D. (2014). *The Cosmological Constant Puzzle: Synergies with Nuclear Physics and its Measurement in Astrophysics Experiments.* Nuclear Physics News, 24:2, 10-1. http://www.tandfonline.com/doi/abs/10.1080/10619127.2014.910427

Bedaque, P.F., Berkowitz, E. and Cherman, A. (2012). *Nuclear Condensate and Helium White Dwarfs*. ApJ, 749(1), 5-13. http://iopscience.iop.org/article/10.1088/0004637X/749/1/5/meta

Bennet, J., Donahue, M., Schneider, N. & Voit, M. (2009). *The Cosmic Perspective*. San Francisco, CA: Addison-Wesley.

Bergeron et al. (2011). *A Comprehensive Spectroscopic Analysis of DB White Dwarfs.* ApJ, 737(1), 28-52.

Carnegie Science. *Magellan Telescopes*. http://obs.carnegiescience.edu/Magellan. Accessed 7 June 2017.

Chamel, N., Haensel, P., Zdunik, J. L., & Fantina, A. F. (2013). *On the Maximum Mass of Neutron Stars*. Int. J. Mod. Phys., E22. https://arxiv.org/abs/1307.3995

Chayer, P. (2013). *Radiative Levitation of Silicon in the Atmospheres of Two Hyades DA White Dwarfs.* MNRAS, 437:L95-L99. https://arxiv.org/pdf/1310.6245.pdf

Cohen, M., Wheaton, Wm. A., Megeath, S. T. (2003). *Spectral Irradiance Calibration in the Infrared. XIV. The Absolute Calibration of 2MASS.* AJ, 126(2): 1090-1096. http://iopscience.iop.org/article/10.1086/376474/pdf

Debes, J. H. et al. (2011). *The WIRED Survey I. A Bright IR Excess Due to Dust Around the Heavily Polluted White Dwarf GALEX J193156.8+011745*. ApJ, 729: 1. http://iopscience.iop.org/article/10.1088/0004-637X/729/1/4/meta

Debes, J. H., Hoard, D. W., Wachter, S., Leisawitz, D. T., & Cohen, M. (2011). *The WIRED Survey II: Infrared Excesses in the SDSS DR7 White Dwarf Catalog.* ApJS, 197(2). http://arxiv.org/abs/1110.6162

Debes, J. H., Hoard, D. W., Farihi, J., Wachter, S., Leisawitz, D. T., & Cohen, M. (2012). *The WIRED Survey III. An Infrared Excess Around the Eclipsing Post-Common Envelope Binary SDSS J030308.35+005443.7*. ApJ, 759: 1. http://iopscience.iop.org/article/10.1088/0004-637X/759/1/37/meta

Debes, J. H. & López-Morales, M. (2008). *A Second Look at the Metal Line Variability of G29-38.* ApJ, 677(1), L43. http://iopscience.iop.org/article/10.1086/587550/fulltext/22539.text.html

Debes, J. H. & Sigurdsson, S. (2002). *Are There Unstable Planetary Systems Around White Dwarfs?* ApJ, 572:556-565. http://iopscience.iop.org/article/10.1086/340291/pdf

Deul, E. (1992). *Deep Near-Infrared Survey of the Southern Sky (DENIS).* NASA Technical Reports. https://ntrs.nasa.gov/archive/nasa/casi.ntrs.nasa.gov/19940017994.pdf

Dye et al. (2006). *The UKIRT Infrared Deep Sky Survey Early Data Release.* MNRAS, 372 (3): 1227-1252. http://adsabs.harvard.edu/abs/2006MNRAS.372.1227D

Farihi, J., Jura., M., & Zuckerman, B. (2009). *Infrared Signatures of Disrupted Minor Planets at White Dwarfs.* ApJ 694: 805-819. https://arxiv.org/abs/0901.0973

Farihi, J., Jura, M., Lee, J. E. & Zuckerman, B. (2010). *Strengthening the Case for Asteroidal Accretion: Evidence for Subtle and Diverse Disks at White Dwarfs.* ApJ, 714:1386-1397. http://iopscience.iop.org/article/10.1088/0004-637X/714/2/1386/pdf

Fazio, G.G. et al. (2004). *The Infrared Array Camera (IRAC) for the Spitzer Space Telescope.* ApJS, 154(1): 10-17. http://adsabs.harvard.edu/abs/2004ApJS..154...10F

Fitzgerald, M. T., Hollow, R., Rebull, L. M., Danaia, L. & McKinnon, D. H. (2014). *A Review of High School Level Astronomy Student Research Projects Over the Last Two Decades*. PASA, 31(e037):1-23. http://adsabs.harvard.edu/abs/2014PASA...31...37F

Girven, J., Gänsicke, B.T., Steeghs, D., & Koester, D. (2011). *DA white dwarfs in Sloan Digital Sky Survey Data Release 7 and a search for infrared excess emission*. MNRAS, 417 (2): 1 210-1235.

Hermes, J. J. et al. (2013). *A New Class of Pulsating White Dwarf of Extremely Low Mass: the Fourth and Fifth Members.* MNRAS, 436 (4): 3573-3580. http://arxiv.org/abs/1310.0013.

Hoard, D. W. (Ed). (2011). *White Dwarf Atmospheres and Circumstellar Environments* (Vol 1). Weinheim, Germany: Wiley-VCH.

Hoard, D. W., Debes, J. H., Wachter, S., Leisawitz, D. T., Cohen, & M. (2013). *The WIRED Survey. IV. New Dust Disks from the McCook & Sion White Dwarf Catalog*. ApJ, 770(1). http://iopscience.iop.org/article/10.1088/0004-637X/770/1/21/pdf

Holberg & Bergeron (2006). *Calibration of Synthetic Photometry Using DA White Dwarfs*. AJ, 132(3), 1221-1233. http://iopscience.iop.org/article/10.1086/505938/pdf

HubbleSite. (2005). *Astronomers Use Hubble to 'Weigh' Dog Star's Companion*. [Press Release]. Retrieved from http://hubblesite.org/newscenter/archive/releases/2005/36/full/

Infrared Science Archive (IRSA) (2016). http://irsa.ipac.caltech.edu/applications/finderchart/

Kaiser, N. et al. (2002). *Pan-STARRS: A Large Synoptic Survey Telescope Array*. Proc. SPIE 4836:154. http://dx.doi.org/10.1117/12.457365

Koester, D., Gänsicke, B. T. & Farihi, J. (2014). *The Frequency of Planetary Debris Around Young White Dwarfs.* A&A, 566:1-20. https://www.aanda.org/articles/aa/abs/2014/06/aa23691-14/aa23691-14.html

Kowalski & Saumon (2006). *Found: The Missing Blue Opacity in Atmosphere Models of Cool Hydrogen White Dwarfs.* ApJ, 651(2): L137-L140.

Kuchner, M. J., Koresko, C. D. & Brown, M. E. (1998). *Keck Speckle Imaging of the White Dwarf G29-38: No Brown Dwarf Companion Detected*. ApJ Lett., 508 (1). http://iopscience.iop.org/article/10.1086/311725/meta

Lang, D., Hogg, D. W., Mierle, K., Blanton, M. & Roweis, S. (2010). *Astrometry.net: Blind Astrometric Calibration of Arbitrary Astronomical Images.* AJ, 139(5):1782-1800. http://adsabs.harvard.edu/abs/2010AJ....139.1782L

Lepine, S. & Shara, M. M. (2005). *A catalog of northern stars with annual proper motions larger than 0.15" (LSPM-NORTH catalog).* AJ, 129: 1483-1522. http://iopscience.iop.org/article/10.1086/427854/pdf

Luyten, W. J & Hughes, H. S. (1980). *Proper motion survey with the forty-eight inch Schmidt telescope. LV. First supplement to the NLTT catalogue*. Minneapolis: University of Minnesota. https://heasarc.gsfc.nasa.gov/w3browse/all/nltt.html

Mathew, A. & Nancy, M. K. (2014). *General Relativistic Calculations for White Dwarf Stars*. http://arxiv.org/abs/1401.0819v2.

Metcalfe, T.S., Montgomery, M.H. and Kanaan, A. (2004). *Testing White Dwarf Crystallization Theory with Asteroseismology of the Massive Pulsating DA Star BPM 37093.* ApJ, 605, L133-L136. http://arxiv.org/abs/astro-ph/0402046

Melis, C. et al. (2011). *Accretion of a Terrestrial-Like Minor Planet by a White Dwarf.* ApJ, 732(2). http://arxiv.org/pdf/1102.0311v1.pdf.

Mizusawa, T., Rebull, L. M., Stauffer, J. R., Bryden, G., Meyer, M., Song, I. (2012). *Exploring the Effects of Stellar Rotation and Wind Clearing: Debris Disks around F Stars,* AJ, 144, 135 http://adsabs.harvard.edu/abs/2012AJ....144..135M

Mustill, A. J., Villaver, E., Veras, D., Bonser, A. & Wyatt, M. C. (2013). *White Dwarf Planets*. EPJ Web of Conferences, 47. http://www.epj-conferences.org/articles/epjconf/pdf/2013/08/epjconf_hpcs2012_06008.pdf

O'Neill, I. (2015, October 21). Caught in the Act: White Dwarf is Killing a Planet. *Discovery News.* http://news.discovery.com/space/astronomy/caught-in-the-act-white-dwarf-is-killing-a-planet-151021.htm.

Persson et al. (2013). PASP, 125, 654. http://instrumentation.obs.carnegiescience.edu/FourStar/Documents/documentation.html

Reach, W. T., Lisse, C., von Hippel, T. & Mullally, F. (2008). *The Dust cloud around the White Dwarf G 29-38.* ApJ, 693(1). http://iopscience.iop.org/article/10.1088/0004-637X/693/1/697/meta

Rebull, L. M. (2012). *More on filters and bandpasses*. http://coolwiki.ipac.caltech.edu/index.php/More_on_filters_and_bandpasses

Rebull, L. M. (2014). *SED Plots*. http://coolwiki.ipac.caltech.edu/index.php/SED_plots

Rebull, L. M. et al. (2015). *On Infrared Excesses Associated With Li-Rich K Giants.* AJ, 150:4. http://iopscience.iop.org/article/10.1088/0004-6256/150/4/123/meta

Rocchetto, M., Farihi, J., Gänsicke, B. T., Bergfors, C. (2014). *The frequency and infrared brightness of circumstellar discs at white dwarfs.* MNRAS, 449 (1): 574-587. http://arxiv.org/abs/1410.6527

Rowell, N. & Hambly, N. C. (2011). *White dwarfs in the SuperCOSMOS Sky Survey: the thin disc, thick disc and spheroid luminosity functions.* MNRAS, 417(1):93-113. http://adsabs.harvard.edu/abs/2011MNRAS.417...93R

Saha, Swapan K. (2007). *Diffraction-Limited Imaging with Large and Moderate Telescopes*. Hackensack, NJ: World Scientific Publishing.

SDSS Collaboration (2015). *The Thirteenth Data Release of the Sloan Digital Sky Survey: First Spectroscopic Data from the SDSS-IV Survey MApping Nearby Galaxies at Apache Point Observatory*. Draft version, https://arxiv.org/pdf/1608.02013.pdf.

Sion, E. M., Greenstein, J. L, Landstreet, J. D., Liebert, J., Shipman, H. L. & Wegner, G. A. (1983). *A Proposed New White Dwarf Spectral Classification System.* ApJ., 269: 253-257. http://adsabs.harvard.edu/abs/1983ApJ...269..253S

Skrutskie et al. (2006). *The Two Micron All Sky Survey (2MASS)*. AJ, 131:1163-1183. http://iopscience.iop.org/article/10.1086/498708/pdf

Steele, P. R., Burleigh, M. R., Dobbie, P. D., Jameson, R. F., Barstow, M. A., Satterthwaite, R. P. (2011). *White dwarfs in the UKIRT Infrared Deep Sky Survey Large Area Survey: the substellar companion fraction*. MNRAS, 416(4): 2768-2791. https://doi.org/10.1111/j.1365-2966.2011.19225.x

Steele, P. R., Burleigh, M. R., Dobbie, P. D., Barstow, M. A. (2007). *Near-infrared Spectroscopy of the Very Low Mass Companion to the Hot DA White Dwarf PG1234+482*. MNRAS, 382(4):1804-1808. https://doi.org/10.1111/j.1365-2966.2007.12481.x

Thorne, Kipp. *Black Holes and Time Warps*. New York: W. W. Norton & Company Inc.

Tremblay, P. E., Bergeron, P. & Giannas, A. (2011). *An Improved Spectroscopic Analysis of DA White Dwarfs from the Sloan Digital Sky Survey Data Release 4*. ApJ, 730(2): 128, 23pp. http://iopscience.iop.org/article/10.1088/0004-637X/730/2/128/pdf

Vanderburg, A. et. al. (2015). *A Disintegrating Minor Planet Transiting a White Dwarf.* Nature, 526:546-549. http://arxiv.org/abs/1510.06387

Vennes, S., Kawka, A. & Nemeth, P. (2011). *Pressure shifts and abundance gradients in the atmosphere of the DAZ white dwarf GALEX J193156.8+011745*. MNRAS, 413(4): 2545-2553. https://doi.org/10.1111/j.1365-2966.2011.18323.x

von Hippel, T., Kuchner, M. J., Kilic, M., Mullally, F. & Reach, W. T. (2007). *The New Class of Dusty DAZ White Dwarfs.* ApJ, 662(1): 544-551. http://adsabs.harvard.edu/abs/2007ApJ...662..544V

Wang, Z., Tziamtzis, A. & Wang. X. (2014). *Near-Infrared Imaging of White Dwarfs With Candidate Debris Disks.* ApJ, 782: 20-26. http://iopscience.iop.org/article/10.1088/0004-637X/782/1/20/pdf

Wenger et al. (2000). *The SIMBAD Astronomical Database.* A&AS, 143:9-22. http://simbad.u-strasbg.fr/simbad/

Werner et al. (2004). *The Spitzer Space Telescope Mission*. APJS, 154:1-9. http://iopscience.iop.org/article/10.1086/422992/pdf

Wilson, D. J. et al. (2014). *Variable emission from a gaseous disc around a metal-polluted white dwarf.* MNRAS, 445(2):1878-1884. https://doi.org/10.1093/mnras/stu1876

Wright, E. L. et al. (2010). *The Wide-field Infrared Survey Explorer (WISE): Mission Description and Initial On-orbit Performance.* AJ, 140:1868-1881. http://iopscience.iop.org/article/10.1088/0004-6256/140/6/1868/pdf

Xu, S. & Jura, M. (2012). *Spitzer Observations of White Dwarfs: the Missing Planetary Debris Around DZ Stars*. ApJ, 745(1): http://adsabs.harvard.edu/abs/2012ApJ...745...88X

Zuckerman, B. (2001). *Dusty Circumstellar Disks*. Annu. Rev. Astron. Astrophys, 39:549-580. http://www.annualreviews.org/doi/abs/10.1146/annurev.astro.39.1.549

Zuckerman, B. & Becklin, E. E. (1987). *Excess infrared radiation from a white dwarf - an orbiting brown dwarf?* Nature, 330. http://adsabs.harvard.edu/abs/1987Natur.330..138Z

Zuckerman, B. & Becklin, E. E. (1992). *Companions to white dwarfs: very low-mass stars and the brown dwarf candidate GD 165B.* ApJ, 386:260-264. http://adsabs.harvard.edu/doi/10.1086/171012

Zuckerman, B., Koester, D., Reid, I. N. & Hünsch, M. (2003). *Metal Lines in DA White Dwarfs.* ApJ, 596: 477-495. http://iopscience.iop.org/article/10.1086/377492/pdf

Zuckerman, B., Melis, C., Klein, B., Koester, D. & Jura, M. (2010). *Ancient Planetary Systems are Orbiting a Large Fraction of White Dwarf Stars.* ApJ, 722:725–736. http://iopscience.iop.org/article/10.1086/377492/pdf

APPENDICES

APPENDIX A

TARGET LIST OF COORDINATES

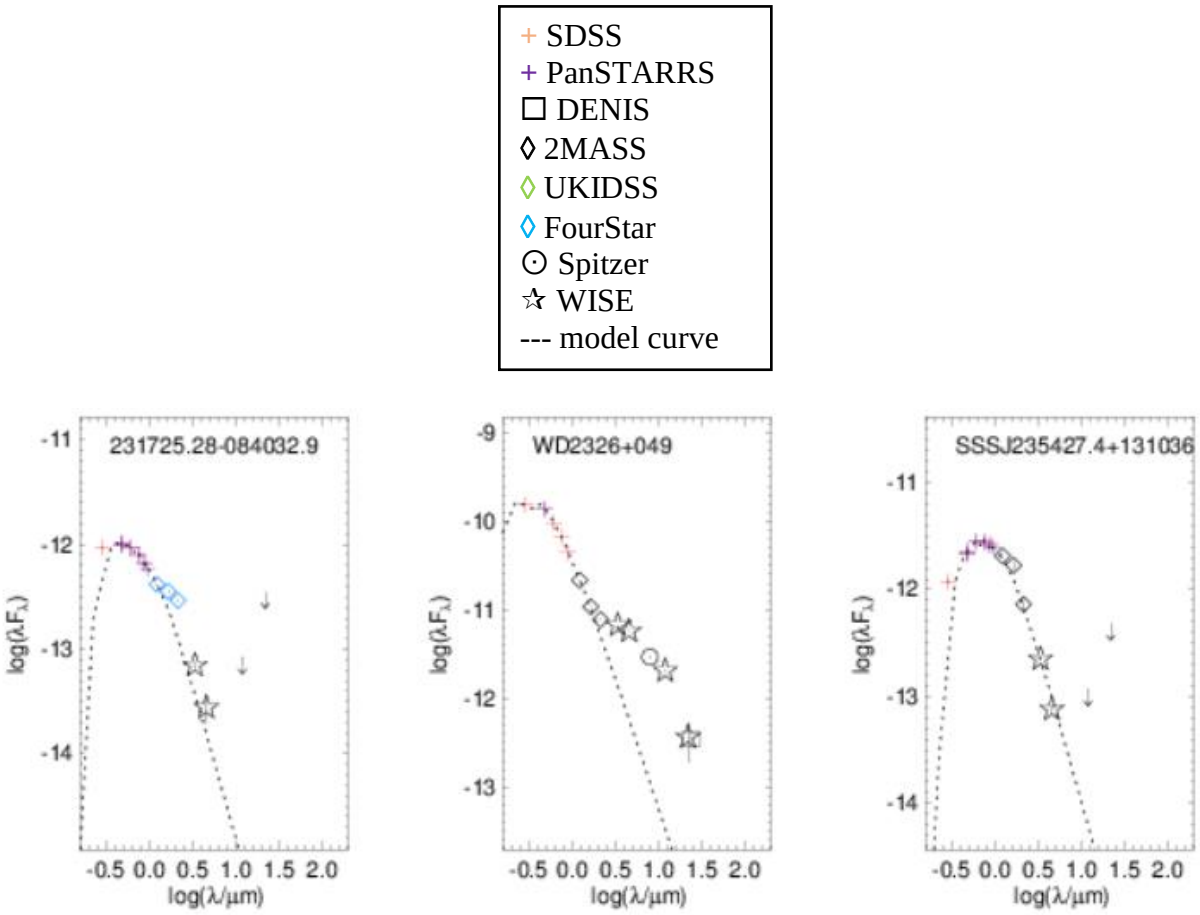
Table 7
Target list with coordinates (N=66)

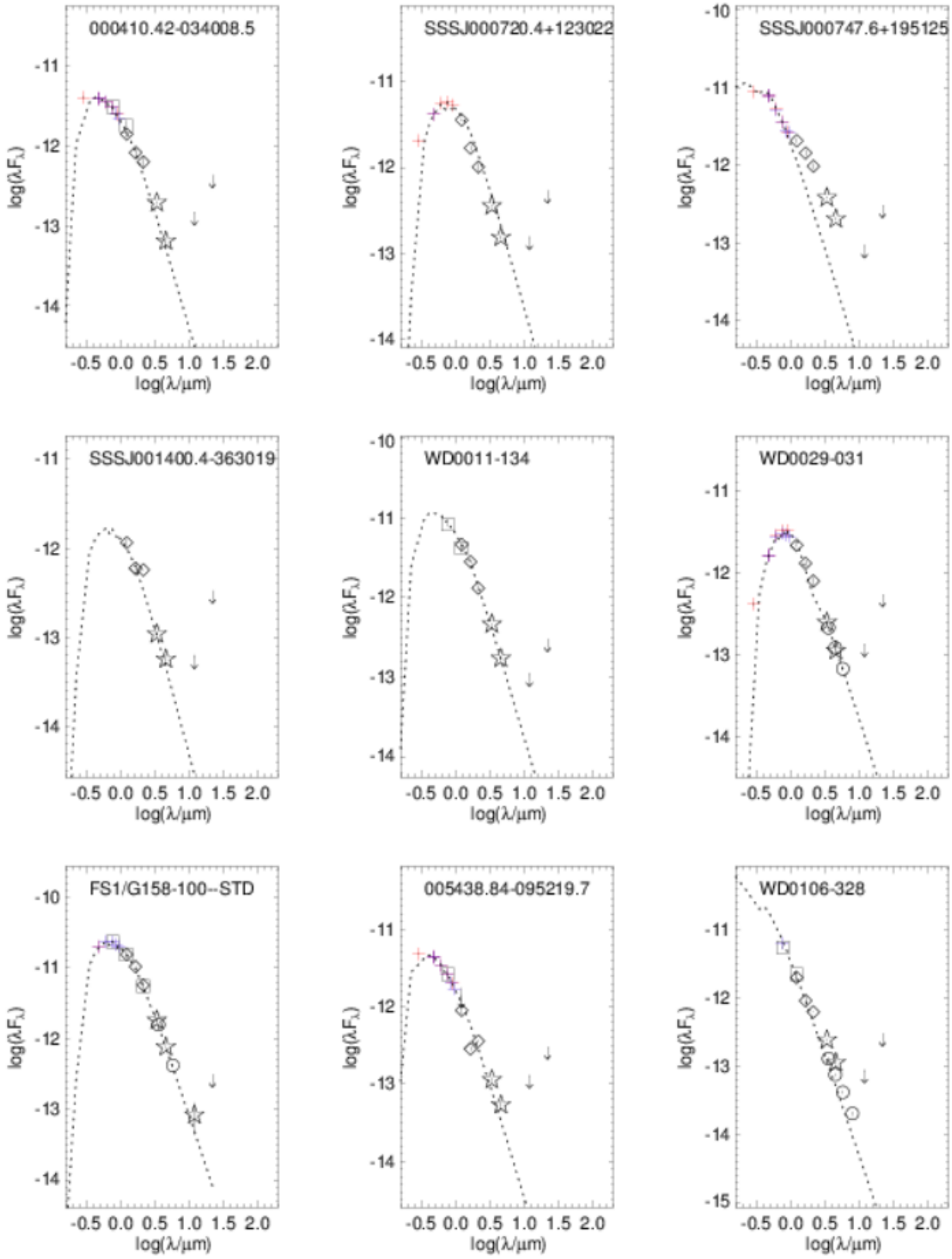
Target name	RA (Degrees)	Dec (Degrees)
000410.42-034008.5	1.043712	-3.66912
005438.84-095219.7	13.66108	-9.87229
011055.05+143922.2	17.73042	14.65596
011616.94-094347.9	19.07047	-9.72989
012532.02+135403.6	21.38339	13.90086
013532.97+144555.9	23.88654	14.76499
124810.23+100541.2	192.0426	10.09466
141632+111003	214.1367	11.16779
143406.75+150817.8	218.5281	15.13832
144847.79+145645.7	222.1991	14.94604
153149.04+025705.0	232.9544	2.951494
154729.96+065909.5	236.8746	6.985963
155359.87+082131.3	238.4995	8.358705
155409.03+172124.1	238.5378	17.35664
160153.23+273547.1	240.4718	27.59687
160715.8+1314312.3	241.8158	13.72009
160839.52+172336.9	242.1645	17.3938
161717.04+162022.3	244.3212	16.33945
163233.0+085125	248.1393	8.855441
164216.62+225627.8	250.5691	22.94081
172920.9-085409.4	262.3377	-8.90391
174246.5-650515	265.6957	-65.0869
174343.8-742437.4	265.9292	-74.4108
183708.5-765905	279.2836	-76.9853
183751.2-725310	279.4624	-72.8871
200348.8-474758	300.9531	-47.8008
222030.69-004107.3	335.1278	-0.68576
222416.84-161534.7	336.0725	-16.2633
230645.72+212859.3	346.6906	21.48318
231725.28-084032.9	349.3553	-8.67607
FS-1/G158-100	8.477437	-12.1335
FS-34	310.6446	-20.0766
GD153	194.2597	22.03102

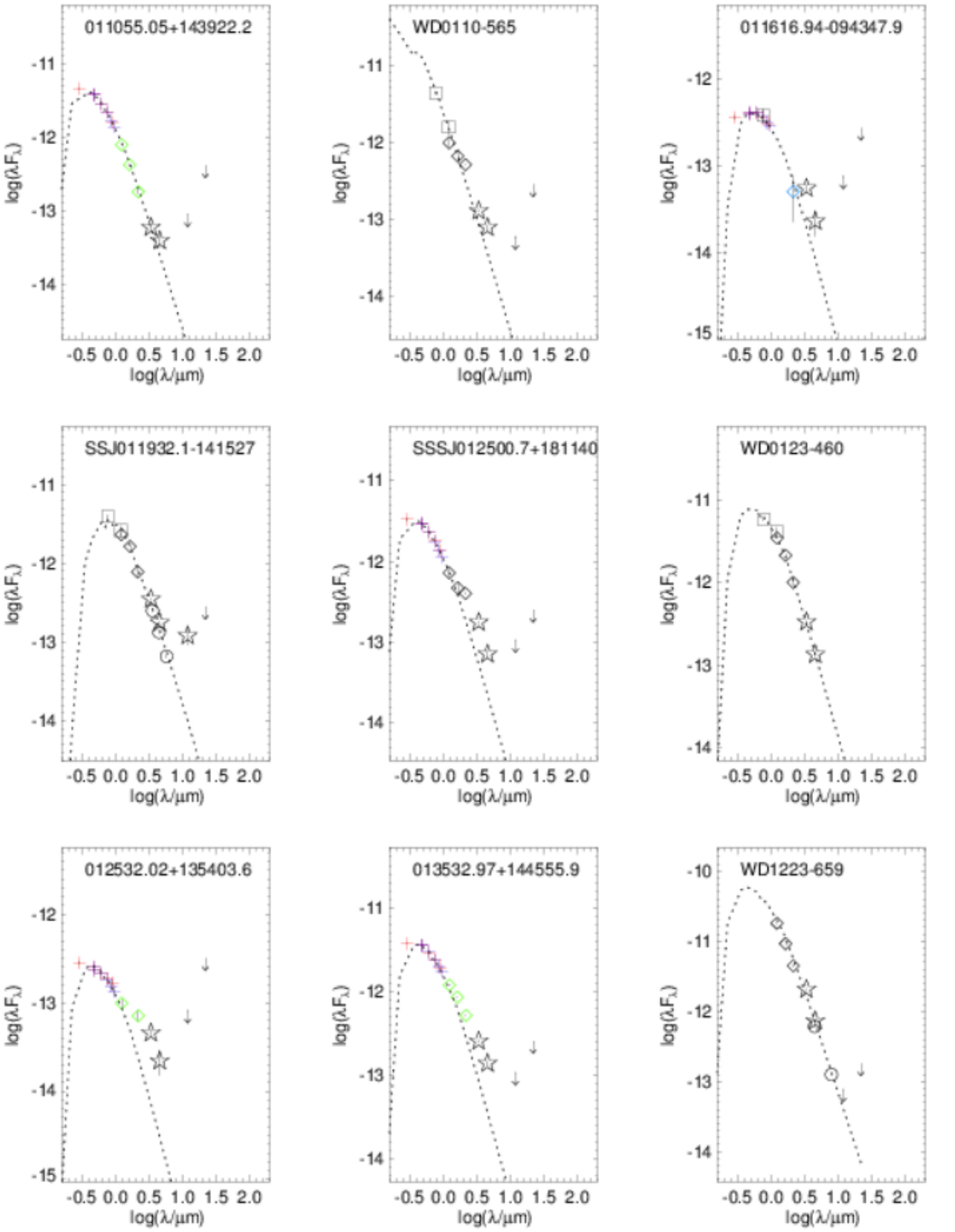
Target name	RA (Degrees)	Dec (Degrees)
J2209+1222	332.3952	12.39353
J224626.38-005909.2	341.6098	-0.98596
LDS749B	323.0681	0.25403
J011932.1-141527	19.88257	-14.2587
J000747.6+195125	1.948431	19.85684
J001400.4-363019	3.501737	-36.5054
J012500.7+181140	21.25241	18.19465
J142439.3+091716	216.1624	9.286761
J161338.8-051960	243.41	-5.33326
J182139.0+144159	275.4126	14.69941
J201017.5-214644	302.5734	-21.7805
J222001.0-741850	335.003	-74.3144
J222125.3-412525	335.3561	-41.4245
J224324.9-262260	340.8543	-26.3833
J231153.3+163719	347.9724	16.62197
J231222.7+161555	348.0945	16.26419
J235427.4+131036	358.6142	13.17673
PG 1457-086	224.971	-8.82506
WD0011-134	3.5533	-13.1836
WD0029-031	8.043414	-2.89986
WD0106-328	17.15008	-32.6287
WD0110-565	18.08798	-56.241
WD0123-460	21.32512	-45.7586
WD1223-659	186.6749	-66.2058
WD1456+298	224.5272	29.62415
WD1919+145	290.4182	14.67806
WD1919+145	290.4182	14.67806
WD1929+012	292.9871	1.295567
WD2115-560	319.903	-55.8371
WD2118-388	320.524	-38.6431
WD2152-548	329.089	-54.6397
WD2326+049	352.1984	5.24834
J1557+0916	239.3365	9.273461

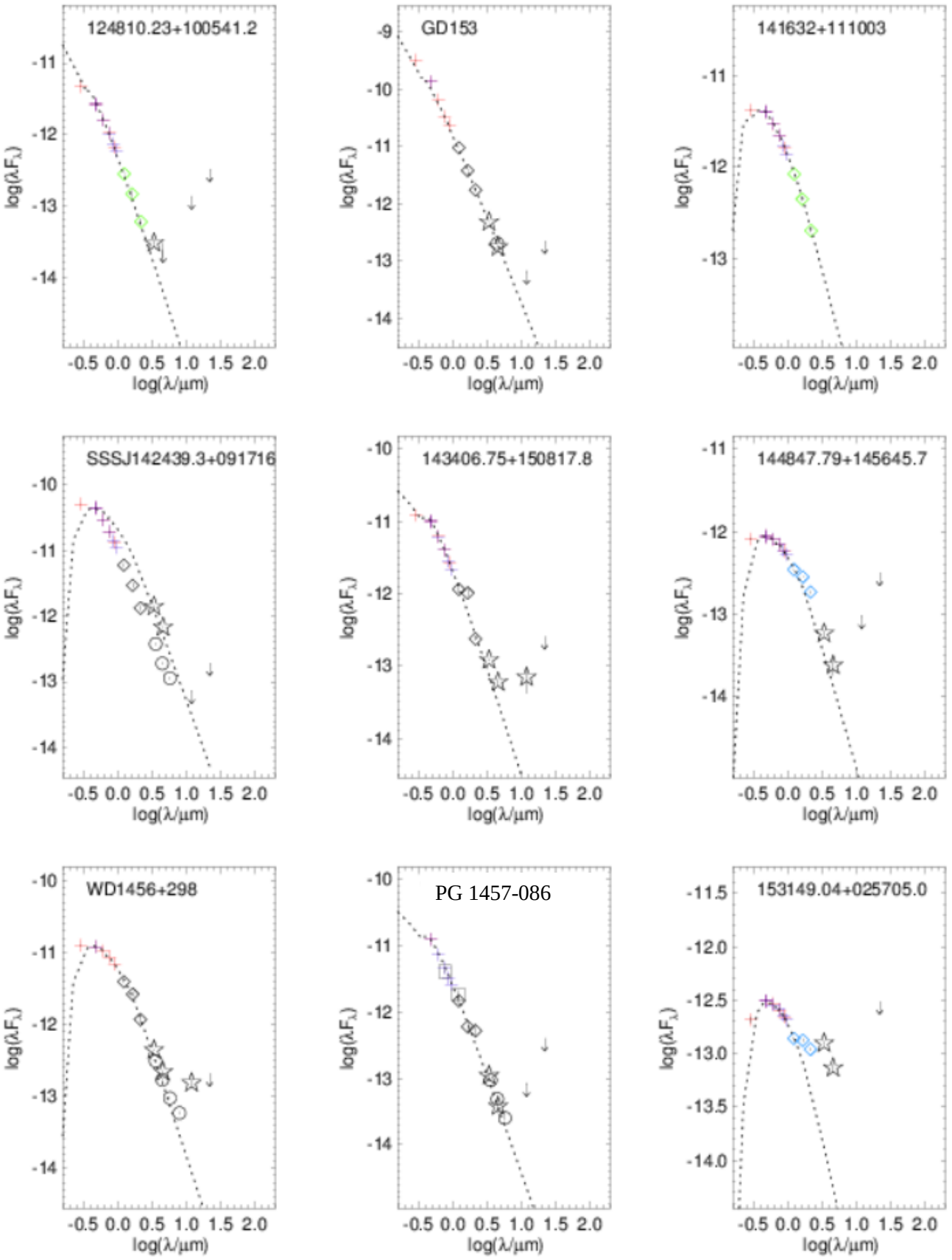
APPENDIX B

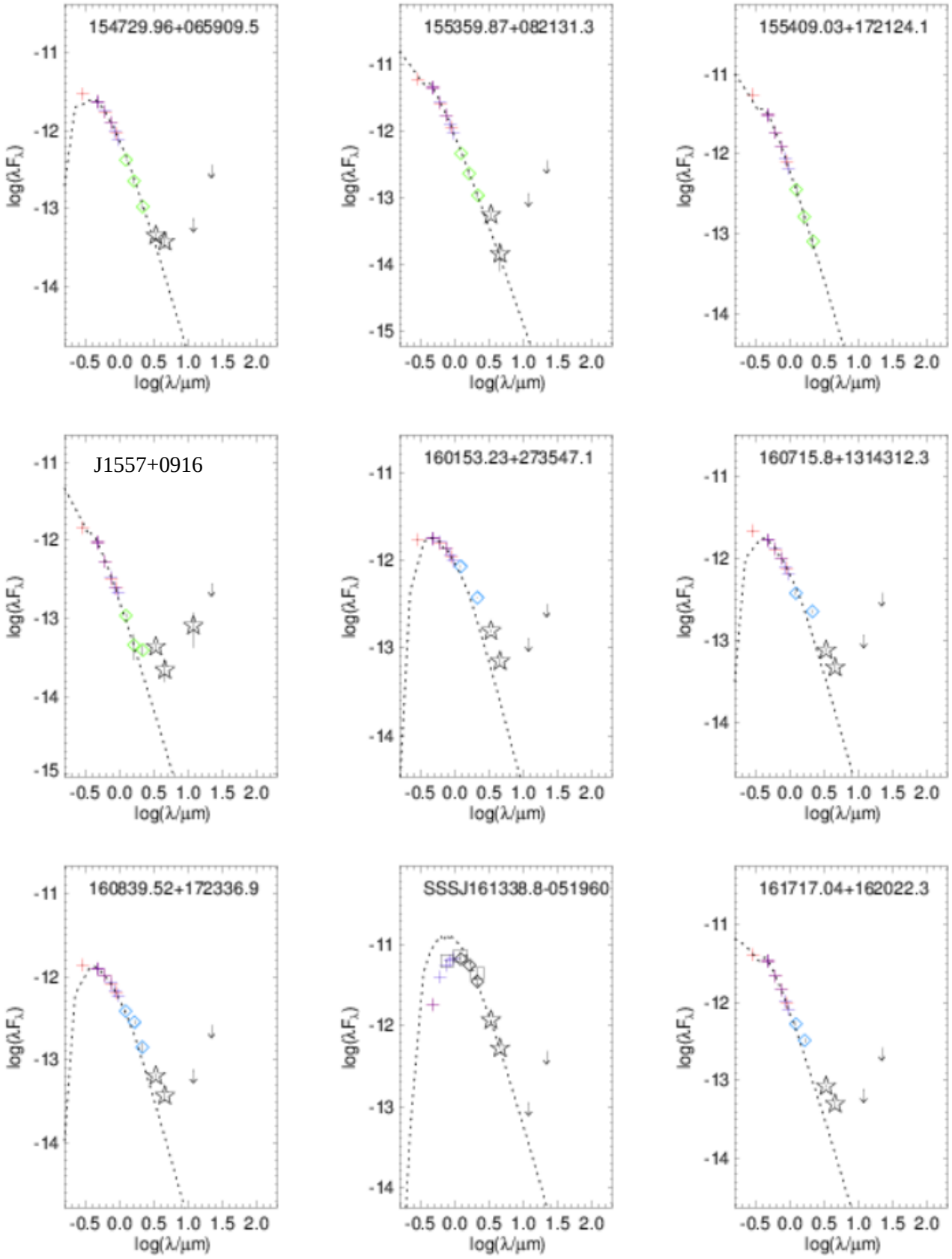
SEDs

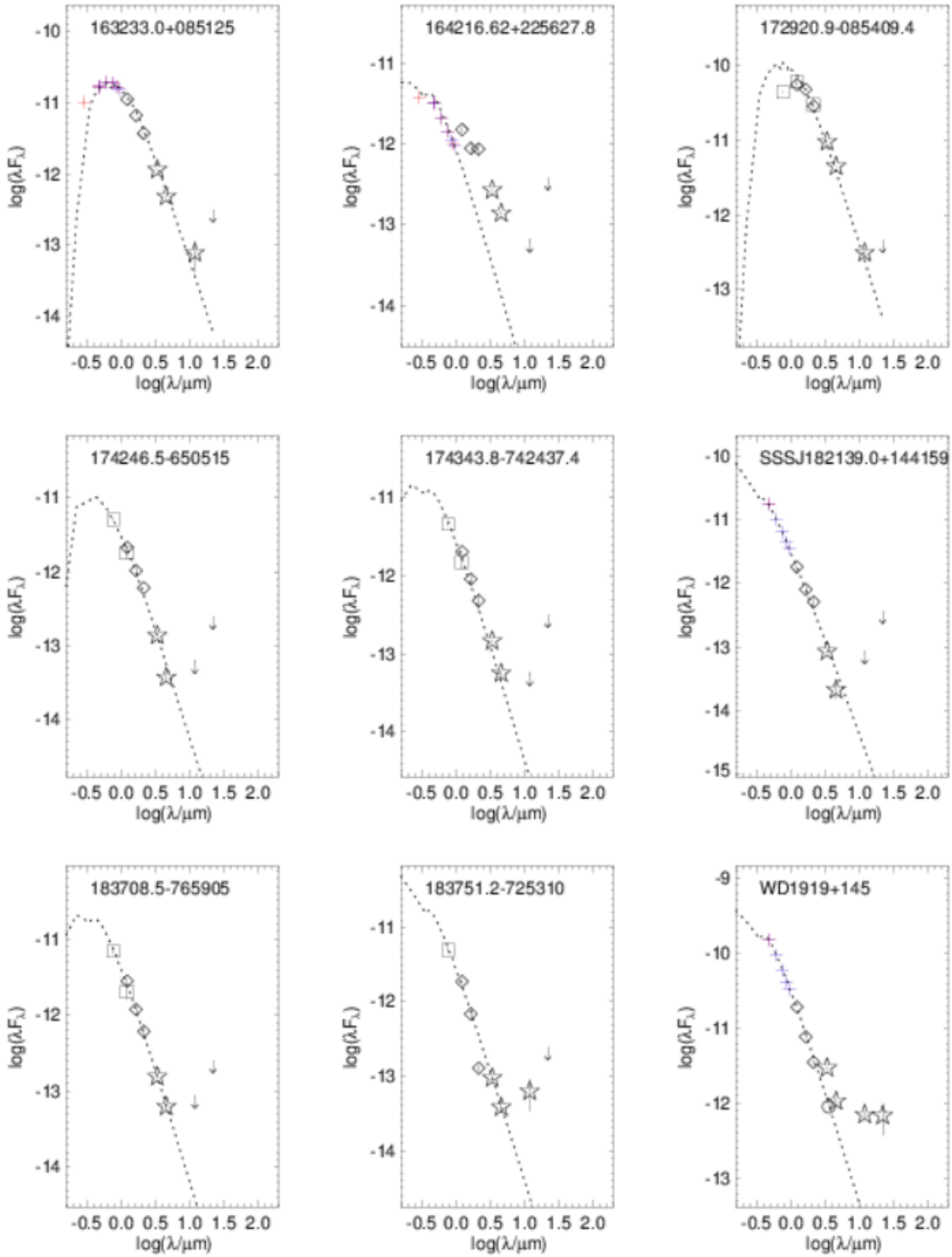

+ SDSS
+ PanSTARRS
☐ DENIS
◊ 2MASS
◊ UKIDSS
◊ FourStar
⊙ Spitzer
☆ WISE
--- model curve
231725.28-084032.9
WD2326+049
SSSJ235427.4+131036
log(λF_λ)
log(λ/μm)

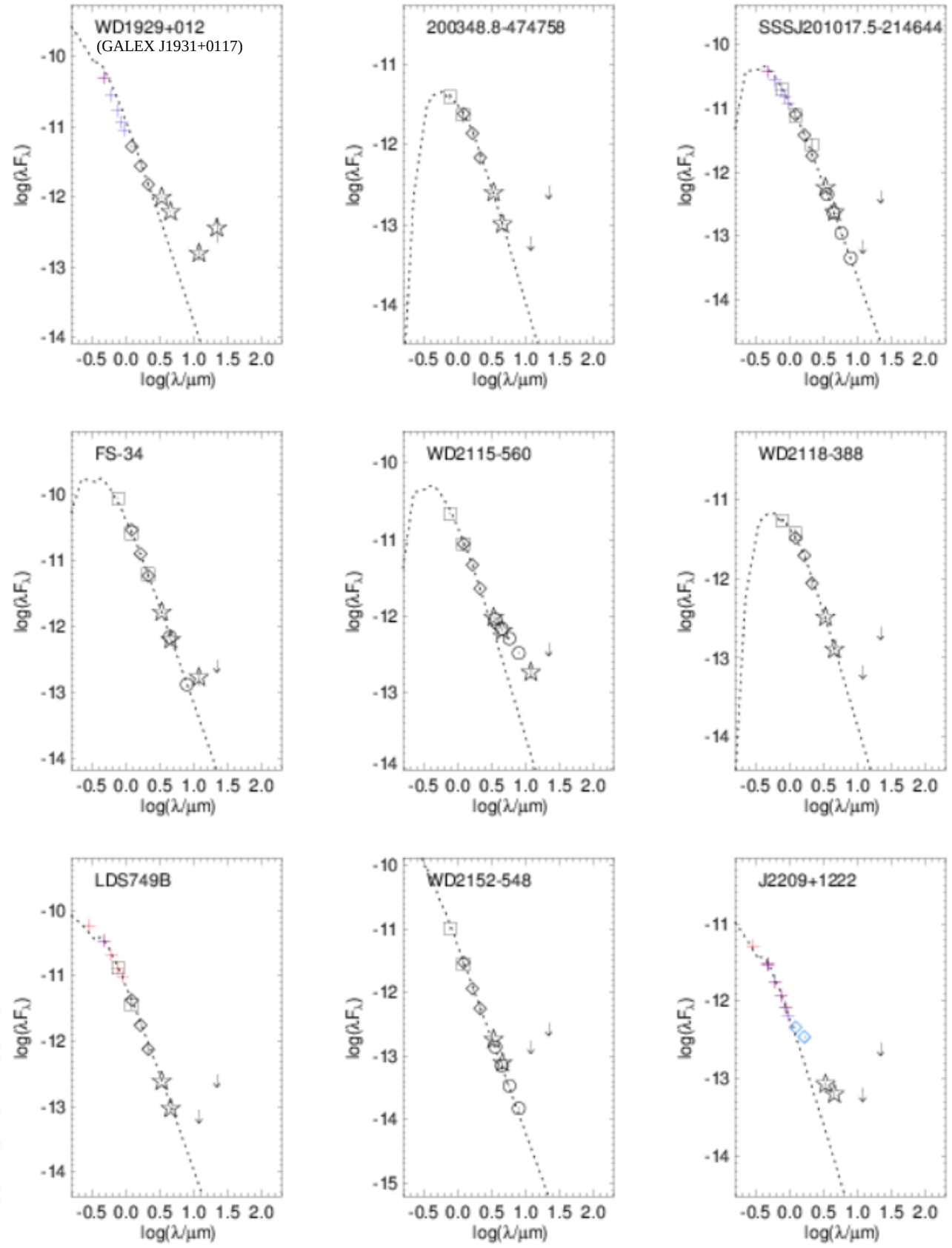

000410.42-034008.5
SSSJ000720.4+123022
SSSJ000747.6+195125
SSSJ001400.4-363019
WD0011-134
WD0029-031
FS1/G158-100--STD
005438.84-095219.7
WD0106-328
log(λF_λ)
log(λ/μm)

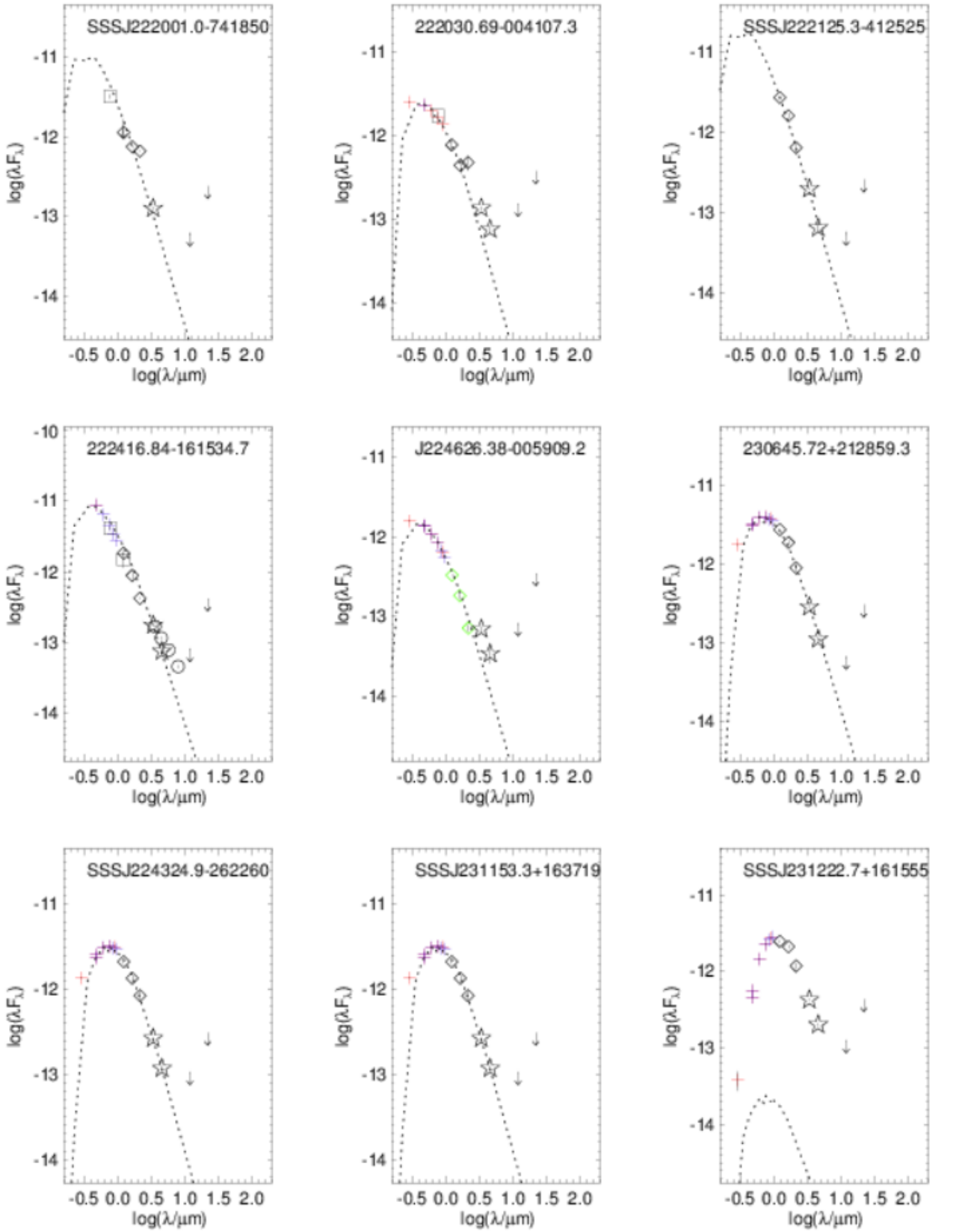

011055.05+143922.2
WD0110-565
011616.94-094347.9
SSJ011932.1-141527
SSSJ012500.7+181140
WD0123-460
012532.02+135403.6
013532.97+144555.9
WD1223-659
log(λF_λ)
log(λ/μm)


124810.23+100541.2
GD153
141632+111003
SSSJ142439.3+091716
143406.75+150817.8
144847.79+145645.7
WD1456+298
PG 1457-086
153149.04+025705.0
log(λF_λ)
log(λ/μm)


154729.96+065909.5
155359.87+082131.3
155409.03+172124.1
J1557+0916
160153.23+273547.1
160715.8+1314312.3
160839.52+172336.9
SSSJ161338.8-051960
161717.04+162022.3
log(λF_λ)
log(λ/μm)


163233.0+085125
164216.62+225627.8
172920.9-085409.4
174246.5-650515
174343.8-742437.4
SSSJ182139.0+144159
183708.5-765905
183751.2-725310
WD1919+145
log(λF_λ)
log(λ/μm)


WD1929+012
(GALEX J1931+0117)
200348.8-474758
SSSJ201017.5-214644
FS-34
WD2115-560
WD2118-388
LDS749B
WD2152-548
J2209+1222
log(λF_λ)
log(λ/μm)


SSSJ222001.0-741850
222030.69-004107.3
SSSJ222125.3-412525
222416.84-161534.7
J224626.38-005909.2
230645.72+212859.3
SSSJ224324.9-262260
SSSJ231153.3+163719
SSSJ231222.7+161555
log(λF_λ)
log(λ/μm)

APPENDIX C

MODEL PARAMETERS

Table 8
Model Parameters (N=66)

Target	Teff	log(g)	Mass	Age	Distance	χ^2 value
000410.42-034008.5	7163.26	8	0.59	1.41E+09	46.21	16.48
005438.84-095219.7	8632.65	8	0.59	8.64E+08	63.21	9.53
011055.05+143922.2	9204.08	8	0.6	7.62E+08	75.62	14.28
011616.94-094347.9	6306.12	8	0.58	1.92E+09	108.27	10.82
012532.02+135403.6	7448.98	8	0.59	1.27E+09	194.92	16.42
013532.97+144555.9	7816.33	8	0.59	1.12E+09	58.28	122.65
124810.23+100541.2	20673.47	8	0.63	6.32E+07	215.59	114.05
141632+111003	9204.08	8	0.59	7.34E+08	75.58	22.19
143406.75+150817.8	14224.49	8	0.62	2.36E+08	81.7	19.1
144847.79+145645.7	6836.73	8	0.59	1.58E+09	88.58	11.53
153149.04+025705.0	6469.39	8	0.58	1.82E+09	134.03	105.99
154729.96+065909.5	9653.06	8	0.6	6.74E+08	104.89	18.42
155359.87+082131.3	15775.51	8	0.61	1.65E+08	135.57	7.41
155409.03+172124.1	15244.9	8	0.62	1.91E+08	155.36	391.5
160153.23+273547.1	7081.63	8	0.59	1.45E+09	66.69	53.23
160715.80+134312.3	8469.39	8	0.6	9.45E+08	97.18	19.23
160839.52+172336.9	8020.41	8	0.6	1.09E+09	100.79	18.14
161717.04+162022.3	13163.26	8	0.6	2.86E+08	132.19	36.68
163233.0+085125	5448.98	8	0.59	3.46E+09	11.8	71.52
164216.62+225627.8	12714.29	8	0.61	3.20E+08	120.93	545.75
172920.9-085409.4	3408.16	8	0.57	1.04E+10	5.17	510.54
174246.5-65051.5	9448.98	8	0.6	7.13E+08	50.36	0.81
174343.8-742437.4	11816.33	8	0.61	3.95E+08	64.91	10.81
183708.5-765905	11571.43	8	0.61	4.18E+08	52.23	1.05
183751.2-725310	15612.24	8	0.62	1.77E+08	74.52	1.26
200348.8-474758	6061.22	8	0.58	2.13E+09	30.15	4.12
222030.69-004107.3	7571.43	8	0.59	1.22E+09	66.83	42.19
222416.84-161534.7	8224.49	8	0.59	9.80E+08	42.07	17.01
230645.72+212859.3	5285.71	8	0.58	4.16E+09	24.8	60.99
231725.28-084032.9	6877.55	8	0.59	1.56E+09	82.62	9.9
FS-1/G158-100	5367.35	8	0.58	3.74E+09	10.35	6.85
FS-34	10836.73	8	0.6	4.80E+08	15.8	7.81
GD153	23857.14	8	0.63	2.93E+07	41.83	1062.7
J2209+1223	15530.61	8	0.62	1.80E+08	158.78	354.6
J224626.38-005909.2	8387.75	8	0.59	9.31E+08	106.33	14.31
LDS749B	13938.78	8	0.62	2.50E+08	43.21	862.58
J011932.1-141527	4714.29	8	0.57	6.80E+09	21.24	12.12

Table 8 continued:
Model Parameters (N=66)

Target	Teff	log(g)	Mass	Age	Distance	χ^2 value
J000720.4+123022	5040.82	8	0.59	5.56E+09	18.62	64.06
J000747.6+195125	12387.75	8	0.6	3.38E+08	81.37	143.29
J001400.4-363019	5653.06	8	0.59	2.90E+09	42.77	0.83
J012500.7+181140	8673.47	8	0.59	8.53E+08	77.8	55.37
J142439.3+091716	7408.16	8	0.59	1.29E+09	14.87	46.56
J161338.8-051960	4918.37	8	0.57	5.99E+09	11.63	109.72
J182139.0+144159	17775.51	8	0.62	1.20E+08	76.01	2.59
J201017.5-214644	9938.77	8	0.59	6.02E+08	26.42	1.5
J222001.0-741850	10510.2	8	0.61	5.38E+08	61.85	7.61
J222125.3-412525	10469.39	8	0.6	5.26E+08	47.23	1.19
J224324.9-262260	20755.1	8	0.63	6.23E+07	100.13	2.08
J231153.3+163719	5081.63	8	0.57	5.22E+09	25.46	9.52
J231222.7+161555	4795.92	8	0.57	6.49E+09	268.08	1
J235427.4+131036	5244.9	8	0.59	4.49E+09	28.13	40.17
PG 1457-086	14306.12	8	0.61	2.24E+08	75.19	1.87
WD0011-134	6959.18	8	0.59	1.51E+09	25.27	1.08
WD0029-031	4061.22	8	0.57	8.84E+09	17.38	78.71
WD0106-328	15530.61	8	0.62	1.80E+08	67.27	58.34
WD0110-565	15163.26	8	0.62	1.94E+08	77.74	12.79
WD0123-460	6632.65	8	0.58	1.71E+09	27.69	0.88
WD1223-659	7367.35	8	0.6	1.36E+09	12.67	16.31
WD1456+298	7367.35	8	0.59	1.31E+09	27.72	17.96
WD1919+145	13979.59	8	0.6	2.40E+08	21.12	35.1
WD1929+012	16918.37	8	0.62	1.38E+08	36.94	157.34
WD2115-560	9734.69	8	0.61	6.59E+08	23.88	2.61
WD2118-388	6346.94	8	0.6	1.97E+09	26.79	1.52
WD2152-548	34714.29	8	0.66	6.26E+06	96.68	1.74
WD2326+049	11285.71	8	0.61	4.46E+08	17.44	3935.2
J1557+0916	18551.02	8	0.61	9.84E+07	339.96	18.29